Inorganic Chemistry
Article

Inorg. Chem. **2009**, *48*, 8771–8783 **8771**
DOI: 10.1021/ic900969n

Iron(III) Complexes of Tripodal Monophenolate Ligands as Models for Non-Heme Catechol Dioxygenase Enzymes: Correlation of Dioxygenase Activity with Ligand Stereoelectronic Properties

Ramasamy Mayilmurugan,[†] Kusalendiran Visvaganesan,[†] Eringathodi Suresh,[‡] and Mallayan Palaniandavar*[,†]

[†]*School of Chemistry, Bharathidasan University, Tiruchirapalli 620 024, India, and* [‡]*Analytical Science Discipline, Central Salt and Marine Chemicals Research Institute, Bhavnagar − 364 002, India*

Received May 19, 2009

The iron(III) complexes $[Fe(L)Cl_2]$ **1**−**6** of the tripodal monophenolate ligands *N,N*-bis(2-pyridylmethyl)-*N*′-(2-hydroxybenzyl)amine H(L1), [(1-methylimidazol-2-ylmethyl)-(pyrid-2-ylmethyl)aminomethyl]-phenol H(L2), 2,4-dimethyl-6-[(1-methylimidazol-2-ylmethyl)(pyrid-2-ylmethyl)aminomethyl]phenol H(L3), *N,N*-dimethyl-*N*′-(pyrid-2-ylmethyl)-*N*′-(2-hydroxybenzyl)ethylenediamine H(L4), *N,N*-dimethyl-*N*′-(1-methylimidazol-2-ylmethyl)-*N*′-(2-hydroxybenzyl)ethylenediamine H(L5), and *N,N*-dimethyl-*N*′-(1-methylimidazol-2-ylmethyl)-*N*′-(2-hydroxy-3,5-dimethylbenzyl)ethylenediamine H(L6) have been isolated and studied as structural and functional models for the intradiol-cleaving catechol dioxygenase enzymes. The complexes have been characterized using elemental analysis, electrospray ionization mass spectrometry, and absorption spectral and electrochemical methods. The single crystal X-ray structures of $[Fe(L3)Cl_2]$ **3** and $[Fe(L6)Cl_2]$ **6** have been successfully determined, and the rhombically distorted octahedral coordination geometry around iron(III) in them are constituted by the phenolate oxygen and pyridyl/-NMe_2, and *N*-methylimidazolyl and tertiary amine nitrogens of the tripodal tetradentate ligands H(L3)/H(L6) and two cis-coordinated chloride ions. The sterically demanding -NMe_2 group as in **6** imposes an Fe−O−C bond angle (139.8°) and Fe−O bond length (1.852 Å), which are very close to those (Fe−O−C, 133, 148°; Fe−O(tyrosinate), 1.81, 1.91 Å) of 3,4-PCD enzymes. The Fe−O−C bond angle observed for **6** is higher than that for **3** (125.1°), and the Fe−O(phenolate) bond distance in **6** is shorter than that in **3** (1.905 Å). In methanol solution all the complexes exhibit two phenolate-to-Fe(III) ligand-to-metal charge transfer (LMCT) bands in the ranges 536−622 and 329−339 nm. Further, when 3,5-di-*tert*-butylcatechol (H_2DBC) pretreated with two moles of Et_3N is added to **1**−**6**, two new intense DBC^{2-}-to-iron(III) LMCT bands (466−489, 676−758 nm) are observed, which are similar to those observed for 3,4-PCD enzyme−substrate complex. All the complexes elicit oxidative intradiol cleavage of H_2DBC in the presence of O_2. Interestingly, among the present complexes, **3** containing coordinated *N*-methylimidazolyl nitrogen shows the highest rate of intradiol cleavage, which correlates with the highest energy of DBC^{2-}-to-iron(III) LMCT band and the most negative $DBSQ/DBC^{2-}$ redox potential. Also, the catecholate adducts of complexes **4** and **5**, both containing a -NMe_2 donor group, react faster and produce higher amounts of intradiol cleavage products (**4**: 55.3; **5**, 50.6%) than the analogous complexes **1** (43.2%) and **2** (32.7%), both containing a pyridyl nitrogen donor, which is consistent with the more negative $DBSQ/DBC^{2-}$ redox potentials for **4** and **5**. The increase in rate of catechol dioxygenation with increase in the DBC^{2-}-to-iron(III) LMCT band energy and decrease in $DBSQ/DBC^{2-}$ redox potential is illustrated by invoking a facile α-electron transfer from iron(III) to catecholate-bound molecular oxygen in the substrate activation mechanism proposed for the intradiol-cleaving catechol dioxygenases. Also, when the substituents on the phenolate arm are varied to tune the Lewis acidity of iron(III) center, the reaction rate decreases with decrease in Lewis acidity and, interestingly, extradiol cleavage is also observed when the Lewis acidity is decreased further by incorporating a 3,5-dimethylphenolate arm as in **6**.

Introduction

Several mononuclear non-heme iron enzymes activate dioxygen to catalyze key biochemical transformations, including many of medical, pharmaceutical, and environmental significance.[1] They are divided into two general groups: substrate activating and dioxygen activating enzymes.[2] The substrate activating enzymes, which include lipoxygenases

*To whom correspondence should be addressed. E-mail: palaniandavarm@gmail.com, palanim51@yahoo.com.

(1) (a) Que, L., Jr. In *Bioinorganic Catalysis*, 2nd ed.; Reedijk, J., Ed.; Marcel Dekker: New York) 1993; pp 347−393. (b) Krüger, H.-J. *Biomimetic Oxidations Catalyzed By Transition Metal Complexes*; Meunier, B., Ed.; Imperial College: London, 2000; pp 363−413.
(2) Neidig, M. L.; Solomon, E. I. *Chem. Commun.* **2005**, 5843–5863.

Published on Web 08/20/2009

and intradiol dioxygenases, are characterized by their utilizing high-spin iron(III) sites to activate organic substrates for direct reaction with dioxygen. The two most investigated enzymes of the intradiol dioxygenases are catechol 1,2-dioxygenase (1,2-CTD) and protocatechuate 3,4-dioxygenase (3,4-PCD). The latter is one of the most extensively studied intradiol dioxygenases, and it catalyzes the ring cleavage of 3,4-dihydroxybenzoate (protocatechuate, PCA) to form β-carboxy-*cis*,*cis*-muconate, with the incorporation of both the oxygen atoms of molecular oxygen between the vicinal hydroxyl groups of the substrate.[3−9] The X-ray crystal structure of 3,4-PCD reveals a trigonal bipyramidal iron(III) active site with four endogenous protein ligands (Tyr408, Tyr447, His460, and His462) and a solvent-derived ligand, and upon substrate binding, the active site geometry is converted into a square-pyramidal geometry with the axial Tyr447 and equatorial OH^- being displaced by the doubly deprotonated substrate (Scheme 1).[10−12] The open coordination position

Scheme 1. Structures of Active Site of 3,4-PCD (A) and the 3,4-PCD-Substrate Adduct (B)

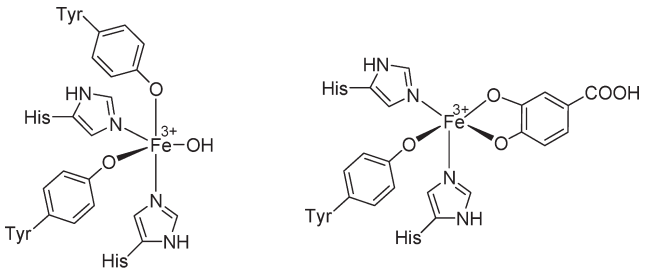

(A) (B)

is *trans* to His460, and the substrate chelates asymmetrically to the iron(III) center, with the longer bond *trans* to the equatorial Tyr408.[11] In contrast to the intradiol dioxygenases, the extradiol dioxygenases utilize iron(II) in the active site with a square pyramidal coordination geometry constituted by two histidine, one glutamate, and two water molecules.[13−15]

Several iron(III) complexes of tri- and tetradentate tripodal 4N ligands[16−26] have been isolated and studied as synthetic analogues for the active sites of the intradiol-cleaving catechol dioxygenase enzymes. Although the tyrosine residues in the intradiol-cleaving 3,4-PCD enzymes play a very vital role in stabilizing the active site geometries and dictating the enzyme functions, only a few synthetic iron(III) complexes of phenolate ligands have been isolated and studied to reproduce the structure and function of the enzymes.[27−34]

(3) Ohlendorf, D. H.; Lipscomb, J. D.; Weber, P. C. *Nature* **1988**, *336*, 403–405.
(4) Ohlendorf, D. H.; Orville, A. M.; Lipscomb, J. D. *J. Mol. Biol.* **1994**, *244*, 586–608.
(5) Valley, M. P.; Brown, C. K.; Burk, D. L.; Vetting, M. W.; Ohlendorf, D. H.; Lipscomb, J. D. *Biochemistry* **2005**, *44*, 11024–11039.
(6) Frazee, R. W.; Orville, A. M.; Dolbeare, K. B.; Yu, H.; Ohlendorf, D. H.; Lipscomb, J. D. *Biochemistry* **1998**, *37*, 2131–2144.
(7) Vetting, M. W.; D' Argenio, D. A.; Ornston, L. N.; Ohlendorf, D. H. *Biochemistry* **2000**, *39*, 7943–7955.
(8) Vetting, M. W.; Ohlendorf, D. H. *Structure* **2000**, *8*, 429–440.
(9) Elgren, T. E.; Orville, A. M.; Kelly, K. A.; Lipscomb, J. D.; Ohlendorf, D. H.; Que, L., Jr. *Biochemistry* **1997**, *36*, 11504–11513.
(10) Whittaker, J. W.; Lipscomb, J. D.; Kent, T. A.; Munck, E.; Orme-Johnson, N. R.; Orme-Johnson, W. H. *J. Biol. Chem.* **1984**, *259*, 4487–4495. Orville, A. M.; Lipscomb, J. D. *J. Biol. Chem.* **1989**, *264*, 8791–8801. True, A. E.; Orville, M.; Pearce, L. L.; Lipscomb, J. D.; Que, L., Jr. *Biochemistry* **1990**, *29*, 10847–10854.
(11) Orville, A. M.; Lipscomb, J. D.; Ohlendorf, D. H. *Biochemistry* **1997**, *36*, 10052–10066.
(12) (a) Orville, A. M.; Elango, N.; Lipscomb, J. D.; Ohlendorf, D. H. *Biochemistry* **1997**, *36*, 10039–10051. (b) Horsman, G. P.; Jirasek, A.; Vaillancourt, F. H.; Barbosa, C. J.; Jarzecki, A. A.; Xu, C. L.; Mekmouche, Y.; Spiro, T. G.; Lipscomb, J. D.; Blades, M. W.; Turner, R. F. B.; Eltis, L. D. *J. Am. Chem. Soc.* **2005**, *127*, 16882–16891.
(13) Siegbahn, P. E. M.; Haeffner, F. *J. Am. Chem. Soc.* **2004**, *126*, 8919–8932.
(14) Miller, M. A.; Lipscomb, J. D. *J. Biol. Chem.* **1996**, *271*, 5524–5535.
(15) Kovaleva, E. G.; Lipscomb, J. D. *Science* **2007**, *316*, 453–456.
(16) Costas, M.; Mehn, M. P.; Jensen, M. P.; Que, L., Jr. *Chem. Rev.* **2004**, *104*, 939–986.
(17) Abu-Omar, M.; Loaiza, A.; Hontzeas, N. *Chem. Rev.* **2005**, *105*, 2227–2252.
(18) (a) Lauffer, R. B.; Heistand, R. H., II; Que, L., Jr. *J. Am. Chem. Soc.* **1981**, *103*, 3947–3949. (b) Heistand, R. H., II; Roe, A. L.; Que, L., Jr. *Inorg. Chem.* **1982**, *21*, 676–681. (c) Heistand, R. H., II; Lauffer, R. B.; Fikrig, E.; Que, L., Jr. *J. Am. Chem. Soc.* **1982**, *104*, 2789–2796. (d) Lauffer, R. B.; Heistand, R. H., II; Que, L., Jr. *Inorg. Chem.* **1983**, *22*, 50–55. (e) White, L. S.; Nilsson, P. V.; Pignolet, L. H.; Que, L., Jr. *J. Am. Chem. Soc.* **1984**, *106*, 8312–8313. (f) Pyrz, J. W.; Roe, A. L.; Stern, L. J.; Que, L., Jr. *J. Am. Chem. Soc.* **1985**, *107*, 614–620. (g) Que, L., Jr.; Kolanczyk, R. C.; White, L. S. *J. Am. Chem. Soc.* **1987**, *109*, 5373–5380. (h) Funabiki, T.; Sakamoto, H.; Yoshida, S.; Tarama, K. *J. Chem. Soc., Chem. Commun.* **1979**, 754–755. (i) Funabiki, T.; Yamazaki, T.; Fukui, A.; Tanaka, T.; Yoshida, S. *Angew. Chem., Int. Ed.* **1998**, *37*, 513–515. (j) Ogo, S.; Yamahara, R.; Funabiki, T.; Masuda, H.; Watanabe, Y. *Chem. Lett.* **2001**, 1062–1063. (k) Funabiki, T.; Fukui, A.; Hitomi, Y.; Higuchi, M.; Yamamoto, T.; Tanaka, T.; Tani, F.; Naruta, Y. *J. Inorg. Biochem.* **2002**, *91*, 151–158. (l) Funabiki, T.; Sugio, D.; Inui, N.; Maeda, M.; Hitomi, Y. *Chem. Commun.* **2002**, 412–413. (m) Hitomi, Y.; Higuchi, M.; Tanaka, T.; Funabiki, T. *Inorg. Chim. Acta* **2005**, *358*, 3465–3470. (n) Higuchi, M.; Hitomi, Y.; Minami, H.; Tanaka, T.; Funabiki, T. *Inorg. Chem.* **2005**, *44*, 8810–8821. (o) Lim, J. H.; Lee, H. -J.; Lee, K. -B.; Jang, H. G. *Bull. Korean Chem. Soc.* **1997**, *18*, 1166–1171. (p) Bruijnincx, P. C. A.; Lutz, M.; Spek, A. L.; Hagen, W. R.; van Koten, G.; Klein Gebbink, R. J. M. *Inorg. Chem.* **2007**, *46*, 8391–8402. (q) Li, F.; Wang, M.; Li, P.; Zhang, T.; Sun, L. *Inorg. Chem.* **2007**, *46*, 9364–9371.
(19) Yamahara, R.; Ogo, S.; Masuda, H.; Watanabe, Y. *J. Inorg. Biochem.* **2002**, *88*, 284–294.
(20) Jang, H. G.; Cox, D. D.; Que, L., Jr. *J. Am. Chem. Soc.* **1991**, *113*, 9200–9204.
(21) (a) Viswanathan, R.; Palaniandavar, M. *J. Chem. Soc., Dalton Trans.* **1995**, 1259–1266. (b) Viswanathan, R.; Palaniandavar, M.; Balasubramanian, T.; Muthiah, P. T. *Inorg. Chem.* **1998**, *37*, 2943–2951. (c) Dhanalakshmi, T.; Bhuvaneshwari, M.; Palaniandavar, M. *J. Inor. Biochem.* **2006**, *100*, 1527–1534. (d) Palaniandavar, M.; Velusamy, M.; Mayilmurugan, R. *J. Chem. Sci.* **2006**, *118*, 601–610. (e) Palaniandavar, M.; Mayilmurugan, R. *C. R. Chim.* **2007**, *10*, 366–379.
(22) Velusamy, M.; Mayilmurugan, R.; Palaniandavar, M. *J. Inorg. Biochem.* **2005**, *99*, 1032–1042.
(23) (a) Pascaly, M.; Duda, M.; Rompel, A.; Sift, B. H.; Klaucke an, W. M.; Krebs, B. *Inorg. Chim. Acta* **1999**, *291*, 289–299. (b) Pascaly, M.; Nazikkol, C.; Scweppe, F.; Wiedeman, A.; Zurlinden, K.; Muller.; Krebs, B. *Z. Anorg. Allg. Chem.* **2000**, *626*, 50–55. (c) Duda, M.; Pascaly, M.; Krebs, B. *J. Chem. Soc., Chem. Commun.* **1997**, 835–836. (d) Merkel, M.; Pascaly, M.; Krebs, B.; Astner, J.; Foxon, S. P.; Schindler, S. *Inorg. Chem.* **2005**, *44*, 7582–7589. (e) Merkel, M.; Schindler, D.; Baldeau, S. M.; Krebs, B. *Eur. J. Inorg. Chem.* **2004**, *44*, 783–790.
(24) Pascaly, M.; Duda, M.; Schweppe, F.; Zurlinden, F.; Muller, K.; Krebs, B. *J. Chem. Soc., Dalton Trans.* **2001**, 828–837.
(25) Koch, W. O.; Krüger, H. -J. *Angew. Chem., Int. Ed. Engl.* **1995**, *34*, 2671–2674.
(26) Cox, D. D.; Benkovic, S. J.; Bloom, L. M.; Bradley, F. C.; Nelson, M. J.; Que, L., Jr.; Wallick, D. E. *J. Am. Chem. Soc.* **1988**, *110*, 2026–2032.
(27) Velusamy, M.; Palaniandavar, M.; Srinivasa Gopalan, R.; Kulkarni, G. U. *Inorg. Chem.* **2003**, *42*, 8283–8293.
(28) Velusamy, M.; Mayilmurugan, R.; Palaniandavar, M. *Inorg. Chem.* **2004**, *43*, 6284–6293.
(29) Merkel, M.; Müller, F. K.; Krebs, B. *Inorg. Chim. Acta* **2002**, *337*, 308–316.
(30) Cox, D. D.; Que, L., Jr. *J. Am. Chem. Soc.* **1988**, *110*, 8085–8092.
(31) Mayilmurugan, R.; Suresh, E.; Palaniandavar, M. *Inorg. Chem.* **2007**, *46*, 6038–6049.
(32) Wang, C.-H.; Lu, J.-W.; Wei, H.-H.; Takeda, M. *Inorg. Chim. Acta* **2007**, *360*, 2944.
(33) Mialane, P.; Anxolabehere-Mallart, E.; Blondin, G.; Nivorojkine, A.; Guilhem, J.; Tchertanova, L.; Cesario, M.; Ravi, N.; Bominaar, E.; Girerd, J.-J.; Münck, E. *Inorg. Chim. Acta* **1997**, *263*, 367.
(34) Yamahara, R.; Ogo, S.; Watanabe, Y.; Funabiki, T.; Jitsukawa, K.; Masuda, H.; Einaga, H. *Inorg. Chim. Acta* **2000**, *300-302*, 587.

Scheme 2. Structures of Sterically Hindered Mono- and Bis(phenolate) Ligands Used in This Study

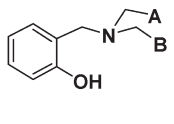

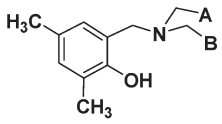

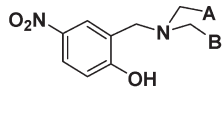

H(L1) A = B = -py
H(L2) A = -py, B = -MeIm
H(L4) A = -py, B = $-CH_2NMe_2$
H(L5) A = -MeIm, B = $-CH_2NMe_2$
H(L3) A = -py, B = -MeIm
H(L6) A = $-CH_2NMe_2$, B = -MeIm
H(L9) A = -py, B = $-CH_2NMe_2$
H_2(L12) A = $-CH_2NMe_2$, B = $-(Me_2)PhOH$
H(L7) A = -py, B = $-CH_2NMe_2$
H(L8) A = -MeIm, B = $-CH_2NMe_2$
H(L10) A = B = -py
H_2(L11) A = $-CH_2NMe_2$, B = $-(NO_2)PhOH$

Que et al. found that incorporation of a phenolate donor in the iron(III) complex of a tripodal 4N ligand led to an extremely lower rate of dioxygenation.[30] We have investigated several iron(III)-monophenolate complexes of linear tridentate and tripodal tetradentate ligands[21] to understand the effect of phenolate and pyridyl/benzimidazolyl donors on the spectral and electrochemical properties and intradiol cleavage yields. Very recently, we have reported[28,31] several iron(III) complexes of tripodal monophenolate ligands with a sterically hindering $-NMe_2$ group, which very closely mimic the stereochemical features such as the $Fe-O_{tyrosinate}$ bond distances (1.81, 1.91 Å) and the Fe−O−C bond angles (133, 148°) in 3,4-PCD enzyme and elicit intradiol cleavage of catechol. Also, the iron(III) complex of a tripodal monophenolate ligand containing pyridylmethyl, 3,5-dimethylphenolate, and sterically hindering $-NMe_2$ arms elicits both intradiol and extradiol cleavages.[31] Also, we have studied a few iron(III) complexes of tripodal and linear bis(phenolate) ligands and one of them containing a $-NMe_2$ donor group exhibits, interestingly, a trigonal bipyramidal iron(III) coordination geometry[27] as in the 3,4-PCD enzymes, but it fails to cleave catechols. Now, we have observed that iron(III) complexes of linear diazapane-based bis-phenolate ligands elicit intradiol cleavage, as well as effect oxidation of catechol to give benzoquinone.[35] However, to date no attempt has been made to systematically study the reactivity of iron(III)-monophenolate complexes and correlate it with their structural, spectral, and electrochemical properties.

All these observations prompted us to design new sterically hindering monophenolate ligands to closely mimic the enzyme active site structure and function of catechol dioxygenases. This article describes the results of our study on the structure, spectra, redox, and dioxygenase activity of iron(III) complexes of systematically varied monophenolate ligands H(L1)−H(L6) (Scheme 2) containing *N*-methylimidazolyl/pyridyl pendant with or without the sterically demanding $-NMe_2$ group, to mimic the amino acid residues tyrosine and histidine in the active site of 3,4-PCD enzyme. Indeed, the X-ray crystal structures of two of the complexes have been determined and one of them with an $-NMe_2$ donor group exhibits Fe−O−C bond angle and Fe−O bond length which are close to those of the enzymes. This is interesting as the Fe−O−C bond angle of equatorially bound tyrosinate in the 3,4-PCD enzyme−substrate complex dictates[36] the asymmetric binding of the chelated substrate moiety via a strong *trans* influence and determines the extent of iron(III)-catecholate covalency and hence the substrate activation for reaction with O_2. Also, it is remarkable that incorporation of electron-releasing $-NMe_2$ group in octahedral iron(III)-phenolate complexes leads to enhanced intradiol cleavage rates, as well as increased amounts of cleavage products. Also, incorporation of electron-releasing but sterically less hindering *N*-methylimidazolyl donor moiety confers enhanced intradiol cleavage rates but with decreased yields of cleavage products. Further, it is remarkable that incorporation of both the electron-releasing *N*-methylimidazolyl and the $-NMe_2$ groups imposes a higher Fe−O−C bond angle and increased regioselective extradiol cleavage products with decreased rate of cleavage.

Experimental Section

Materials. *N,N*-Dimethylethylenediamine, bis(2-pyridylmethyl)amine, 3,5-di-*tert*-butylcatechol (H_2DBC), 4-*tert*-butylcatechol (H_2TBC), 2,4-dimethylphenol, 2-pyridinecarboxaldehyde, sodium cyanotrihydroborate, catechol (H_2CAT) and 4-nitrocatechol (H_2NCAT) (Aldrich), iron(III) chloride (anhydrous) and formaldehyde (37%) (Merck, India), 3,4,5,6-tetrachlorocatechol (H_2TCC, Lancaster), 3-methylcatechol (3-H_2MCAT) and 4-methylcatechol (4-H_2MCAT) (Acros Organics), 2-hydroxybenzaldehyde (Loba, India) were used as received, unless noted otherwise, and H_2DBC was recrystallized from hexane before use. The supporting electrolyte *tetra-N*-butylammonium perchlorate (NBu_4ClO_4, G. F. Smith, U.S.A.) was recrystallized twice from aqueous ethanol.

Physical Measurements. Elemental analyses were performed on a Perkin-Elmer Series II CHNS/O Analyzer 2400. ^{1}H NMR spectra were recorded on a Bruker 200 MHz NMR spectrometer. The electronic spectra were recorded on an Agilent diode array-8453 spectrophotometer. The EPR spectra were recorded on a JEOL JES-TE 100 X-band spectrometer in frozen methanol solution. Electrospray ionization mass spectrometry (ESI-MS) was performed on a Thermo Finnigan LCQ 6000 Advantage Max instrument. Cyclic voltammetry (CV) and differential pulse voltammetry (DPV) were performed using a three electrode cell configuration. A platinum sphere, a platinum plate, and Ag(s)/Ag^+ were used as working, auxiliary, and reference electrodes, respectively. The supporting electrolyte used was NBu_4ClO_4 (TBAP). The temperature of the electrochemical cell was maintained at 25 ± 0.2 °C by a cryocirculator (HAAKE D8 G). By bubbling research grade nitrogen the solutions were deoxygenated, and an atmosphere of nitrogen was maintained over the solutions during measurements. The $E_{1/2}$ values were observed under identical conditions for various scan rates. The instruments utilized included an EG & G PAR 273 Potentiostat/Galvanostat and Pentium-IV computer along with EG & G M270 software to carry out the experiments and to acquire the data. The product analyses were performed using a HP 6890 GC series Gas Chromatograph equipped with a FID detector and a HP-5 capillary column (30 m × 0.32 mm × 2.5 μm) and GC-MS analysis was performed on a Perkin-Elmer Clarus 500 GC-MS instrument using a PE-5 with the previously[28] reported temperature program.

Synthesis of Ligands. *N,N*-Bis(2-pyridylmethyl)-*N*-(2-hydroxybenzyl)amine H(L1). To a solution of 2-hydroxybenzaldehyde (0.61 g, 5 mmol) in methanol (50 mL) were added

(35) Mayilmurugan, R. PhD Thesis, Bharathidasan University, India.
(36) Davies, M. I.; Orville, A. M.; Neese, F.; Zaleski, J. M.; Lipscomb, J. D.; Solomon, E. I. *J. Am. Chem. Soc.* **2002**, *124*, 602–614.

bis(2-pyridylmethyl)amine (1.0 g, 5 mmol) and a small amount of acetic acid. Sodium cyanotrihydroborate (0.31 g, 5 mmol) in methanol (5 mL) was added dropwise to the resulting solution with stirring. After the solution was stirred for 3 days at 25 °C, it was acidified by adding HCl and then evaporated almost to dryness under reduced pressure. The residue was dissolved in saturated aqueous Na_2CO_3 solution (25 mL) and extracted with $CHCl_3$ (3 × 50 mL). The combined extracts were dried over anhydrous Na_2SO_4 and filtered. The filtrate on evaporation gave the ligand H_2(L1) as a colorless oil, which was used for preparation of the complex. Yield: 1.23 g (86%). ^{1}H NMR (200 MHz, $CDCl_3$): δ 8.46−8.48 (m, 4H), 7.55−7.70 (m, 4H), 7.11−7.29 (m, 2H), 6.64−6.85 (m, 2H), 3.78 (s, 4H), 3.70 (s, 2H).

[(1-Methylimidazol-2-ylmethyl)(pyrid-2-ylmethyl)aminomethyl]-phenol H(L2). This was synthesized in two steps. The first step was the preparation of (1-methylimidazol-2-ylmethyl)(pyrid-2-ylmethyl)amine, which was then reacted with 2-hydroxybenzaldehyde and sodium cyanotrihydroborate as reducing agent in the second step to obtain H(L2).

Step 1. (1-Methylimidazol-2-ylmethyl)(pyrid-2-ylmethyl)-amine was prepared by the reaction of 2-aminomethylpyridine (2.0 g, 10 mmol) and *N*-methylimidazol-2-carboxaldehyde (1.65 g, 10 mmol) in methanol (50 mL). After stirring for 24 h $NaBH_4$ (0.57 g, 15 mmol) was added with stirring at 0 °C. The resulting solution was stirred overnight and then the solvent was evaporated. The resulting product was dissolved in water, and the organic layer was extracted with CH_2Cl_2 and dried with Na_2SO_4. The filtrate was evaporated to dryness under reduced pressure to give (1-methylimidazol-2-ylmethyl)(pyrid-2-ylmethyl)amine as pale yellow oil. ^{1}H NMR (200 MHz, $CDCl_3$) δ 7.14−8.55 (m), 6.93 (d, 1H), 6.81 (d, 1H), 3.94 (s, 2H), 3.90 (s, 2H), 3.67 (s, 3H).

Step 2. This step was carried out by using the procedure employed for H(L1) but by using (1-methylimidazol-2-ylmethyl)(pyrid-2-ylmethyl)amine instead of bis(2-pyridylmethyl)amine. Yield: 1.03 g (83%). ^{1}H NMR (200 MHz, $CDCl_3$): δ 8.56−8.57 (m, 2H), 7.61−7.66 (m, 2H), 7.06−7.23 (m, 2H), 6.75−6.94 (m, 2H), 6.89 (d, 1H), 6.72 (d, 1H), 3.86 (s, 2H), 3.73 (s, 2H), 3.72 (s, 2H), 3.40 (s, 3H).

2,4-Dimethyl-6-[(1-methylimidazol-2-ylmethyl)(pyrid-2-ylmethyl)aminomethyl]-phenol H(L3). (1-Methylimidazol-2-ylmethyl)(pyrid-2-ylmethyl)amine (2.18 g, 10.8 mmol) was added to 37% formalin (1.22 g, 16.2 mmol) in methanol (10 mL) at 0 °C under nitrogen, and then 2,4-dimethylphenol (1.32 g, 10.8 mmol) in methanol (8 mL) was added to this dropwise. The solution was allowed to warm up to room temperature and then treated with acetic acid (3 mL). After allowing the mixture to stir for 48 h, the solvent was removed under vacuum, neutralized with dilute NaOH, and extracted three times with CH_2Cl_2. The organic layer was dried over Na_2SO_4, and the solvent was removed under vacuum to get the ligand H(L3) as a viscous oil. The crude product was then purified by passing it over a silica column using CH_2C1_2 as eluent. Yield: 1.28 g (68%). ^{1}H NMR (200 MHz, $CDCl_3$): δ 8.57−8.59 (m, 2H), 7.60−7.66 (m, 2H), 7.16 (s, 1H), 6.73 (s, 1H), 6.84 (d, 1H), 6.70 (d, 1H), 3.76 (s, 2H), 3.71 (s, 2H), 3.62 (s, 2H), 3.41 (s, 3H), 2.27 (s, 3H), 2.22 (s, 3H).

The ligands H(L4)−H(L6) were also synthesized in two steps. The first step involve the preparation of *N,N*-dimethyl-*N*′-(pyrid-2-ylmethyl)ethylenediamine and *N,N*-dimethyl-*N*′-(1-methylimidazol-2-ylmethyl)ethylenediamine, which were then reacted with 2-hydroxybenzaldehyde or 2,4-dimethylphenol using reductive amination or Mannich condensation reaction to yield the ligands H(L4)−H(L6).

***N,N*-Dimethyl-*N*′-(pyrid-2-ylmethyl)ethylenediamine.** *N,N*-Dimethyl-*N*′-(pyrid-2-ylmethyl)ethylenediamine was prepared as reported[22] elsewhere. ^{1}H NMR (200 MHz, $CDCl_3$) δ 7.10−8.51 (pyH), 3.90 (s, 2H), 3.0 (sb, 1H), 2.70 (t, 2H), 2.4 (t, 2H), 2.20 (s, 6H).

***N,N*-Dimethyl-*N*′-(1-methylimidazol-2-ylmethyl)ethylenediamine.** This was prepared by the same method as that used for *N,N*-dimethyl-*N*′-(pyrid-2-ylmethyl)ethylenediamine, except that 1-methyl-2-imidazolecarboxaldehyde was used instead of pyridine-2-carboxaldehyde. The yield was 60%. ^{1}H NMR (200 MHz, $CDCl_3$) δ 6.91 (d, 1H), 6.81 (d, 1H), 3.86 (s, 2H), 3.67 (s, 3H), 2.71 (t, 2H), 2.41 (t, 2H), 2.20 (s, 6H).

***N,N*-Dimethyl-*N*′-(pyrid-2-ylmethyl)-*N*′-(2-hydroxybenzyl)-ethylenediamine (L4).** This ligand was synthesized using the procedure employed for H(L1) but by using *N,N*-dimethyl-*N*′-(pyrid-2-ylmethyl)ethylenediamine instead of bis(pyrid-2-ylmethyl)amine. Yield: 1.26 g (88%). δ 8.44−8.46 (m, 2H), 7.51−7.70 (m, 2H), 7.07−7.19 (m, 2H), 6.70−6.85 (m, 2H), 3.67 (s, 2H), 3.62 (s, 2H), 2.57 (t, 2H), 2.44 (t, 2H), 2.08 (s, 6H).

***N,N*-Dimethyl-*N*′-(1-methylimidazol-2-ylmethyl)-*N*′-(2-hydroxybenzyl)ethylenediamine H(L5).** This ligand was synthesized using the procedure employed for H(L4) but by using *N,N*-dimethyl-*N*′-(1-methylimidazol-2-ylmethyl)ethylenediamine instead of *N,N*-dimethyl-*N*′-(pyrid-2-ylmethyl)ethylenediamine. Yield: 1.18 g (81%). δ 2.02 (s, 6H), 2.43 (t, 2H), 2.54 (t, 2H), 3.13 (s, 3H), 3.46 (s, 2H), 3.50 (s, 2H), 6.66 (d, 1H), 6.71−6.79 (m, 2H), 6.99 (d, 1H), 7.10−7.20 (m, 2H).

***N,N*-Dimethyl-*N*′-(1-methylimidazol-2-ylmethyl)-*N*′-(2-hydroxy-3,5-dimethylbenzyl)ethylenediamine H(L6).** This ligand was synthesized using the procedure employed for the ligand H(L3) but by using *N,N*-dimethyl-*N*′-(1-methylimidazol-2-ylmethyl)ethylenediamine instead of (1-methylimidazol-2-ylmethyl)pyrid-2-ylmethylamine. Yield: 1.26 g (74%). δ 7.19 (s, 1H), 6.81 (s, 1H), 6.80−6.81 (d, 1H), 6.64−6.67 (d, 1H), 3.52 (s, 2H), 3.45 (s, 2H), 3.19 (s, 3H), 2.55 (t, 2H), 2.39 (t, 2H), 2.12 (s, 3H), 2.10 (s, 3H), 2.01 (s, 6H).

Preparation of Complexes. The complexes [Fe(L1)Cl_2] **1**−[Fe(L6)Cl_2] **6** were prepared by reaction of a solution of ferric chloride (0.16 g, 1.0 mmol) in methanol (5 mL) to a methanolic solution (10 mL) of an equivalent amount of the respective ligand H(L) (1.0 mmol) in the presence of an equivalent amount of triethylamine (Et_3N) (0.10 g, 140 μL, 1.0 mmol) in stoichiometric combination. The solution was stirred for an hour to obtain a blue precipitate, which was filtered off, washed with small amounts of cold methanol, and dried in vacuo over P_4O_{10}.

[Fe(L1)Cl_2] 1. Yield, 0.24 g (56%). Anal. Calcd for $C_{19}H_{18}N_3OFeCl_2$: C, 52.93; H, 4.21; N, 9.75%. Found: C, 51.91; H, 4.22; N, 9.78% and confirmed by ESI-MS, $(C_{19}H_{18}N_3OFeCl_2)^+$, *m*/*z*, 431, 396.

[Fe(L2)Cl_2] 2. Yield, 0.32 g (73%). Anal. Calcd for $C_{18}H_{19}N_4OFeCl_2$: C, 49.80; H, 4.41; N, 12.91%. Found: C, 49.89; H, 4.42; N, 12.88% and confirmed by ESI-MS, $(C_{18}H_{19}N_4OFeCl_2)^+$, *m*/*z*, 434, 398.

[Fe(L3)Cl_2] 3. Yield, 0.27 g (58%). Anal. Calcd for $C_{20}H_{23}N_4OFeCl_2$: C, 51.98; H, 5.02; N, 12.12%. Found: C, 51.96; H, 5.10; N, 12.05%. X-ray quality crystals of **3** were obtained by slow evaporation of a methanolic solution of the complex.

[Fe(L4)Cl_2] 4. Yield, 0.26 g (75%). Anal. Calcd for $C_{17}H_{22}N_3OFeCl_2$: C, 49.66; H, 5.39; N, 10.22%. Found: C, 49.69; H, 5.40; N, 10.15% and confirmed by ESI-MS, $(C_{17}H_{22}N_3OFeCl_2)^+$, *m*/*z*, 411, 375.

[Fe(L5)Cl_2] 5. Yield, 0.26 g (64%). Anal. Calcd for $C_{16}H_{22}N_4OFeCl_2$: C, 46.40; H, 5.60; N, 13.53%. Found: C, 46.38; H, 5.62; N, 9.75% and confirmed by ESI-MS, $(C_{19}H_{18}N_3OFeCl_2)^+$, *m*/*z*, 413, 378.

[Fe(L6)Cl_2] 6. Yield, 0.33 g (75%). Anal. Calcd for $C_{18}H_{27}N_4OFeCl_2$: C, 48.89; H, 6.15; N, 15.67% Found: C, 48.90; H, 6.16; N, 12.65%. X-ray quality crystals of **6** were obtained by the slow evaporation of a methanolic solution of the complex.

Kinetics and Product Analysis. Kinetic analysis[20,22−25,27−29] of the catechol cleavage reactions was carried out by time-dependent measurement of the disappearance of the lower

energy catecholate-to-iron(III) ligand-to-metal charge transfer (LMCT) band at ambient temperature (25 °C) by exposing the catecholate adducts generated in situ to molecular oxygen. The solvents were equilibrated at the atmospheric pressure of O_2 at 25 °C, and the solubility of O_2 at 25 °C in methanol is 2.12×10^{-3} M.[24,37] A stock solution of the adduct [Fe(L)(DBC)] was prepared by treating the complexes **1**−**6** (1.0×10^{-2} M) with an equivalent amount of H_2DBC pretreated with 2 equiv of Et_3N. Oxygenation was started by rapid delivery of a stock solution (0.1 mL) of the catecholate adducts (1.0×10^{-2} M) by syringe to O_2-saturated solvent (4.9 mL).

The dioxygenase activities of the present complexes were determined using a known[22−31] procedure with modifications. The catecholate adducts [Fe(L1−L6)(DBC)] of the complexes (0.1 mmol) were generated in situ in methanol solvent (5 mL) and then exposed to dioxygen and stirred for 48 h. The oxygenation reaction was quenched by the addition of 6 M HCl (5 mL), and the products were extracted from the aqueous solution with diethylether (3 × 20 mL). The clear yellow organic layer was separated and dried over anhydrous Na_2SO_4 at room temperature. Further purification of the products was accomplished by column chromatography using silica gel and CH_2Cl_2:CH_3OH (8:1) solvent mixture as eluent. The major products were separated and analyzed by GC, GC-MS, and ^{1}H NMR techniques. The other minor products were analyzed as a mixture, detected by GC-MS (EI), and quantified using GC (FID).

Single Crystal X-ray Data Collection and Structure Solution. The single crystals of **3** and **6** with suitable size were selected from the mother liquor and immersed in paraffin oil, then mounted on the tip of a glass fiber, and cemented using epoxy resin. Intensity data for the crystal were collected using Mo Kα ($\lambda = 0.71073$ Å) radiation on a Bruker SMART APEX diffractometer equipped with CCD area detector at 100 K (**3**) and 293 K (**6**). The crystallographic data are collected in Table 1. The SMART[38] program was used for collecting frames of data, indexing the reflections, and determining the lattice parameters; the SAINT[38] program for integration of the intensity of reflections and scaling; the SADABS[39] program for absorption correction; and the SHELXTL[40] program for space group and structure determination and least-squares refinements on F^2. The structure was solved by the heavy atom method. Other non-hydrogen atoms were located in successive difference Fourier syntheses. The final refinement was performed by full-matrix least-squares analysis. Hydrogen atoms attached to the ligand moiety were located from the difference Fourier map and refined isotropically.

Results and Discussion

Synthesis and Characterization of Ligands and Complexes. The ligands H(L1), H(L2), H(L4), and H(L5) were synthesized by the reductive amination of 2-hydroxybenzaldehyde with the corresponding secondary amine using sodium cyanotrihydroborate as the reducing agent.[41] The ligands H(L3) and H(L6) were synthesized in good yields by the reaction of the Mannich base of 2,4-dimethylphenol formed in situ using excess of 37% aqueous formaldehyde with the corresponding secondary amine.[31] The reaction of $FeCl_3$ and the ligands H(L1)−H(L6) in the presence of Et_3N results in the formation of complexes of the type [Fe(L)Cl_2] in good yields. The formulation of the complexes is based on elemental analysis and ESI-MS and is supported by the X-ray crystal structures of [Fe(L3)Cl_2] **3** and [Fe(L6)Cl_2] **6**. The present tetradentate phenolate ligands containing imidazolyl/pyridyl nitrogen donor are expected to reasonably mimic the histidine and tyrosinate donors in 3,4-PCD enzyme. The bulky *N*,*N*-dimethyl group, the pyridine ring nitrogen, sterically hindered phenolate group, and the more basic *N*-methylimidazole moiety [pK_a (BH^+): imidazole, 6.0; pyridine, 5.2, phenol, 9.95] in the ligands are expected to influence the iron(III) coordination structures as well as the electronic properties of the complexes to provide a systematic variation in Lewis acidity of the iron(III) center and offer steric hindrance to substrate binding so as to closely duplicate the active site in enzyme−substrate complexes. Conductivity measurements reveal that one of the chloride ions in **1**−**6** is quite certainly coordinated in methanol solution (Λ_M, 123−150 Ω^{-1} cm^2 mol^{-1}), and this is confirmed by ESI-MS with all the complexes showing a prominent peak corresponding to the species (methanol) [Fe(L)Cl]$^+$ **1**−**6**: **1**, $(C_{19}H_{18}N_3OFeCl)^+$, *m*/*z*, 396; **2**, $(C_{18}H_{19}N_4OFeCl)^+$, *m*/*z*, 398; **3**, $(C_{20}H_{23}N_4OFeCl)^+$, *m*/*z*, 426; **4**, $(C_{17}H_{22}N_3OFeCl)^+$, *m*/*z*, 375; **5**, $(C_{19}H_{18}N_3OFeCl_2)^+$, *m*/*z*, 378; **6**, $(C_{18}H_{27}N_4OFeCl)^+$, *m*/*z*, 307. The complexes have magnetic moments in the range 5.43−5.96 μ_B at room temperature, which is characteristic of high-spin iron(III).[20−24,27−29] The frozen solution EPR spectra of all the mononuclear iron(III) complexes **1**−**6** display high-spin ($S = 5/2$) rhombic ferric signals[26,42] at $g = 7.00-8.88$, 4.19−4.15, and 1.88−1.93 (E/D, 0.094−0.099) associated with the $|5/2, -1/2\rangle \rightarrow |5/2, +1/2\rangle$ transition and also intense signals corresponding

Table 1. Crystal Data and Structure Refinement for [Fe(L3)Cl_2] and Fe(L6)Cl_2]

	[Fe(L3)Cl_2]	[Fe(L6)Cl_2]
empirical formula	$C_{20}H_{23}Cl_2FeN_4O$	$C_{18}H_{27}Cl_2FeN_4O$
fw	462.18	442.19
crystal system	triclinic	monoclinic
space group	$P\bar{1}$	$P2_1/n$
a (Å)	11.7717(8)	7.187(2)
b (Å)	14.0005(9)	36.435(12)
c (Å)	14.4112(10)	8.394(3)
α (deg)	90.4380(10)	90
β (deg)	111.5970(10)	113.032(5)
γ (deg)	107.8940(10)	90
V (Å^3)	2081.9(2)	2022.9(11)
T (K)	100	293(2)
Mo Kα *λ*, (Å)	0.71073	0.71073
density (Mg m^{-3})	1.475	1.452
Z	4	4
μ (mm^{-1})	0.999	1.024
F(000)	956	924
no. of reflections collected	14746	7837
goodness-of-fit on F^2	1.022	1.200
R1[a]	0.0479	0.1080
wR2[b]	0.1279	0.2364

[a] $R1 = \sum||F_o| - |F_c||/\sum|F_o|$. [b] $wR2 = \{\sum w(F_o^2 - F_c^2)^2/\sum w(F_o^2)^2\}^{1/2}$.

(37) (a) Japan Chemical Society *Kagaku-Binran Basic Part II*, 2nd ed.; Maruzen: Tokyo, Japan, 1975. (b) Sawyer, D. T, *Oxygen Chemistry*; Oxford University Press: New York, 1991.

(38) *SMART & SAINT Software Reference manuals*, version 5.0; Bruker AXS Inc.: Madison, WI, 1998.

(39) Sheldrick, G. M. *SADABS software for empirical absorption correction*; University of Göttingen: Göttingen, Germany, 2000.

(40) *SHELXTL Reference Manual*, version 5.1; Bruker AXS Inc.: Madison, WI, 1998.

(41) Shimazaki, Y.; Huth, S.; Hirota, S.; Yamauchi, O. *Bull. Chem. Soc. Jpn.* **2000**, *73*, 1187–1195.

(42) (a) Fujii, H.; Funahashi, Y. *Angew. Chem., Int. Ed.* **2002**, *41*, 3638–3641. (b) Kurahashi, T.; Oda, K.; Sugimoto, M.; Ogura, T.; Fujii, H. *Inorg. Chem.* **2006**, *45*, 7709–7721.

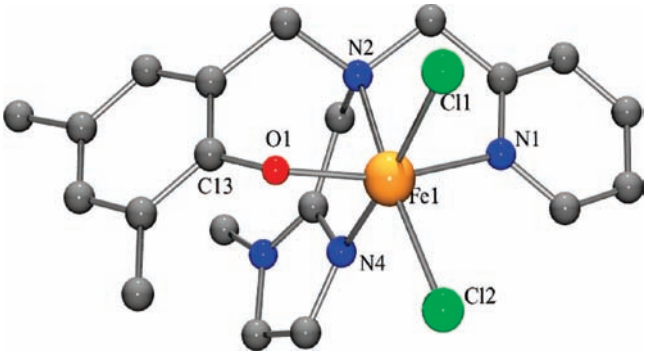

Figure 1. Molecular structure of $[Fe(L3)Cl_2]$ **3** (40% probability factor for the thermal ellipsoid). Hydrogen atoms have been omitted for clarity.

to rhombic low-spin[43,44] ($S = 1/2$) iron(III) species (g, 2.11−2.17). All the complexes display additional signals one at $g = 5.00-5.59$ and two at $g = 1.88-1.99$ in the low field region corresponding to the $|5/2, -3/2\rangle \rightarrow |5/2, +3/2\rangle$ transition.[46,47] The E/D values of the complexes fall in a narrow range revealing that the rhombicity of the complexes is not very much affected by the nature and type of ligand donors. Interestingly, **6** shows a signal at $g = 7.10$, which may correspond to a minor component like solvated species (cf. above).

Description of the Crystal Structures of $[Fe(L3)Cl_2]$ 3 and $[Fe(L6)Cl_2]$ 6. The molecular structure of $[Fe(L3)Cl_2]$ **3** is shown in Figure 1 together with the atom numbering scheme, and the selected bond lengths and bond angles are collected in Table 2. There are two crystallographically independent complex molecules with the same chemical formula present in the asymmetric unit cell, both exhibiting the same coordination geometry but slightly different bond lengths and bond angles. Each one of the two molecules has a FeN_3OCl_2 chromophore constituted by three nitrogen atoms and one phenolate oxygen atom of the tripodal ligand and two chloride ion. The bond angles Cl1−Fe1−N4 (170.42°), O1−Fe1−N1 (160.86°), and Cl2−Fe1−N2 (161.57°) deviate markedly from 180° suggesting distortion of the coordination sphere from ideal octahedron. The $Fe-N_{py}$ (2.213, 2.208 Å) and $Fe-N_{im}$ (2.115, 2.118 Å) bond lengths in both molecules are almost equal and are shorter than the $Fe-N_{amine}$ bond distance (2.280, 2.279 Å), which is expected of the sp^2 and sp^3 hybridizations, respectively, of the pyridyl/imidazolyl and tertiary amine nitrogen atoms.[22,48−50] The $Fe-N_{amine}$ bonds in **3** are longer than the octahedral $Fe^{III}-N_{amine}$ bond (~2.15 Å) observed in other previously[21,23,24,28,29,31,45] reported iron(III) complexes of tripodal tetradentate ligands. The $Fe-O_{phenolate}$ bonds in **3** (1.905 Å) are shorter than the average octahedral $Fe^{III}-O_{phenolate}$ bond distance[24,27−29,31,42] of ~1.98 Å suggesting that the iron−oxygen overlap is stronger and that the Lewis acidity of the iron(III) centers is lower than that in other iron(III)-monophenolate complexes[21,27,28,31] on account of the more Lewis basic 3,5-dimethylphenolate oxygen donor (cf. below). The observed Fe−Cl distances in **3** (2.3218, 2.3141; 2.3031, 2.3379 Å) fall in the range observed for octahedral iron(III) complexes.[21,23,24,27−29,31] Such a difference in bond length of the cis chloride ions would encourage asymmetric chelation of catecholate substrate, which is essential for substrate activation, subsequent reaction with molecular oxygen, and release of products from the reaction intermediate during catalysis.[28,31]

Table 2. Selected Bond Lengths [Å] and Bond Angles [deg] for $[Fe(L3)Cl_2]$ **3**

3a		3b	
Fe(1)−O(1)	1.905(3)	Fe(2)−O(2)	1.903(3)
Fe(1)−N(1)	2.213(4)	Fe(2)−N(5)	2.208(4)
Fe(1)−N(2)	2.280(3)	Fe(2)−N(6)	2.279(3)
Fe(1)−N(4)	2.115(3)	Fe(2)−N(8)	2.118(3)
Fe(1)−Cl(1)	2.3218(10)	Fe(2)−Cl(3)	2.3031(11)
Fe(1)−Cl(2)	2.3141(9)	Fe(2)−Cl(4)	2.3379(9)
Cl(1)−Fe(1)−Cl(2)	98.46(3)	Cl(3)−Fe(2)−Cl(4)	98.67(3)
Cl(1)−Fe(1)−O(1)	93.81(8)	Cl(3)−Fe(2)−O(2)	104.27(8)
Cl(1)−Fe(1)−N(1)	87.49(8)	Cl(3)−Fe(2)−N(5)	94.08(8)
Cl(1)−Fe(1)−N(2)	93.74(8)	Cl(3)−Fe(2)−N(6)	162.21(8)
Cl(1)−Fe(1)−N(4)	170.42(8)	Cl(3)−Fe(2)−N(8)	90.93(8)
Cl(2)−Fe(1)−O(1)	104.36(8)	Cl(4)−Fe(2)−O(2)	94.96(8)
Cl(2)−Fe(1)−N(1)	94.31(8)	Cl(4)−Fe(2)−N(5)	86.93(7)
Cl(2)−Fe(1)−N(2)	161.57(7)	Cl(4)−Fe(2)−N(6)	92.75(7)
Cl(2)−Fe(1)−N(4)	90.68(8)	Cl(4)−Fe(2)−N(8)	169.49(8)
O(1)−Fe(1)−N(1)	160.86(10)	O(2)−Fe(2)−N(5)	161.01(11)
O(1)−Fe(1)−N(2)	88.48(11)	O(2)−Fe(2)−N(6)	88.17(10)
O(1)−Fe(1)−N(4)	86.65(12)	O(2)−Fe(2)−N(8)	86.73(13)
N(1)−Fe(1)−N(2)	72.38(11)	N(5)−Fe(2)−N(6)	72.85(10)
N(1)−Fe(1)−N(4)	88.96(12)	N(5)−Fe(2)−N(8)	88.14(12)
N(2)−Fe(1)−N(4)	76.70(11	N(6)−Fe(2)−N(8)	76.92(10)
Fe(1)−O(1)−C1(3)	125.1(2)	Fe(2)−O(2)−C(33	126.9(2)

The X-ray crystal structure of $[Fe(L6)Cl_2]$ **6** is shown in Figure 2 together with the atom numbering scheme, and the selected bond lengths and bond angles are collected in Table 3. The iron(III) center in the complex molecule has a FeN_3OCl_2 coordination sphere constituted by the phenolate oxygen, imidazole nitrogen, and two tertiary amine nitrogen atoms of the tripodal ligand and two chloride ions occupying the remaining two cis-coordination sites. The distortion in the coordination sphere from ideal octahedron is revealed by the deviation in the N1−Fe1−Cl2 (168.6°), O1−Fe1−N3 (162.6°), and N4−Fe1−Cl1 (166.4°) bond angles from the ideal angle of 180°. The replacement of the pyridyl pendant trans to the phenolate donor in **3** by the sterically demanding -NMe_2 group to obtain **6** results in location of the -NMe_2 group cis to the $Fe-O_{phenolate}$ bond, shortening of the $Fe-O_{phenolate}$ bond to 1.852 Å, and increase in the Fe−O−C bond angle from 125.1, 126.9° in **3** to 139.8° in **6** and the Fe−O−C−C dihedral angle from 125.92° in **3** to 162.78° in **6** (Figure 3). This corresponds to enhanced

(43) (a) Simaan, A. J.; Biollot, M.-L.; Riviere, E.; Boussac, A.; Girerd, J. -J. *Angew. Chem., Int. Ed.* **2000**, *39*, 196–198. (b) Bukowshi, M. R.; Comba, P.; Limberg, C.; Merz, M.; Que, L., Jr.; Wistuba, T. *Angew. Chem., Int. Ed.* **2004**, *43*, 1283–1287.
(44) Yoon, S.; Lee, H. -J.; Lee, K. -B.; Jang, H. G. *Bull. Korean Chem. Soc.* **2000**, *21*, 923–928.
(45) (a) Ito, S.; Suzuki, M.; Kobayashi, T.; Itoh, H.; Harada, A.; Ohba, S.; Nishida, Y. *J. Chem. Soc., Dalton Trans.* **1996**, 2579–2580. (b) Ito, S.; Ishikawa, Y.; Nishino, S.; Kobayashi, T.; Ohba, S.; Nishida, Y. *Polyhedron* **1998**, *17*, 4379–4391.
(46) Korendovych, I. V.; Staples, R. J.; Reiff, W. M.; Rubak-Akimova, E. V. *Inorg. Chem.* **2004**, *43*, 3930.
(47) Bou-Abdallah, F.; Chasteen, N. D. *J. Biol. Inorg. Chem.* **2008**, *13*, 15–24.
(48) (a) Visvaganesan, K.; Mayilmurugan, R.; Suresh, E.; Palaniandavar, M. *Inorg. Chem.* **2007**, *46*, 10294–10306. (b) Sundaravel, K.; Dhanalakshmi, T.; Suresh, E.; Palaniadavar, M. *Dalton Trans.* **2008**, *48*, 7012.
(49) Thomas, K. R. J.; Velusamy, M.; Palaniandavar, P. *Acta Crystallogr.* **1998**, *C54*, 741–743.
(50) Rodriguez, M. C.; Lambert, F.; Morgenstern-Badarau, I.; Cesario, M.; Guilhem, J.; Keita, B.; Nadjo, L. *Inorg. Chem.* **1997**, *36*, 3525–3531.

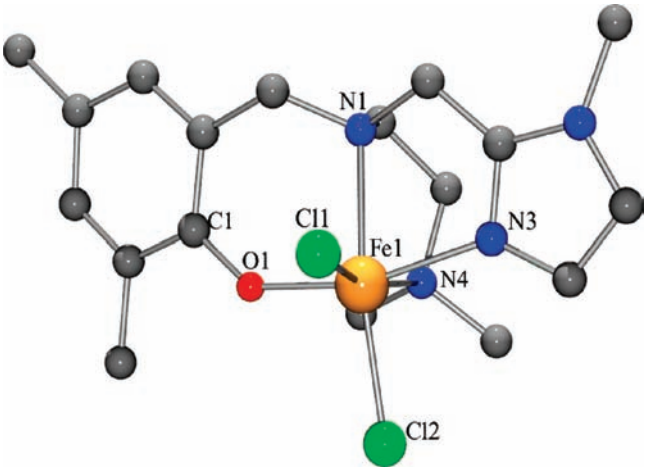

Figure 2. Molecular structure of [Fe(L6)Cl_2] **6** (40% probability factor for the thermal ellipsoid). Hydrogen atoms have been omitted for clarity.

Table 3. Selected Bond Lengths [Å] and Bond Angles [deg] for Fe(L6)Cl_2] **6**

Fe(1)−O(1)	1.852(8)
Fe(1)−N(1)	2.266(9)
Fe(1)−N(3)	2.122(9)
Fe(1)−N(4)	2.317(9)
Fe(1)−Cl(1)	2.371(3)
Fe(1)−Cl(2)	2.288(3)
O(1)−Fe(1)−N(3)	162.6(3)
O(1)−Fe(1)−N(1)	86.1(3)
N(3)−Fe(1)−N(1)	76.6(3)
O(1)−Fe(1)−Cl(2)	98.4(2)
N(3)−Fe(1)−Cl(2)	98.2(3)
N(1)−Fe(1)−Cl(2)	168.6(3)
O(1)−Fe(1)−N(4)	92.3(4)
N(3)−Fe(1)−N(4)	82.2(3)
N(1)−Fe(1)−N(4)	78.7(3)
Cl(2)−Fe(1)−N(4)	90.5(3)
O(1)−Fe(1)−Cl(1)	96.2(3)
N(3)−Fe(1)−Cl(1)	86.6(3)
N(1)−Fe(1)−Cl(1)	91.2(3)
Cl(2)−Fe(1)−Cl(1)	98.71(13)
N(4)−Fe(1)−Cl(1)	166.4(3)
C(1)−O(1)−Fe(1)	139.8(7)

π-back bonding involving the dπ orbitals of iron(III) and the relatively low-lying π^* orbital (vs phenolate ion)[21b] of the weakly σ-bonding phenolate, leading to a stronger Fe−O bond. The Fe−O−C bond angle (139.8°) is almost close to that of 3,4-PCD enzyme[10,36] (Fe−O−C, 133 (equatorial), 148° (axial)), but is higher than those in **3** and other previously reported octahedral iron(III)-phenolate[21,27,28] complexes suggesting the importance of the steric demand imposed by the -NMe_2 group.[28,31] This is interesting as the complexes [Fe(L7)Cl_2] **7** and [Fe(L9)Cl_2] **9**, both containing a -NMe_2 group, exhibit higher Fe−O−C bond angles (**7**, 136.1; **9**, 134.0°, Figure 3). So, it is expected that the complexes **4** and **5** containing a -NMe_2 group also exhibit a higher Fe−O−C bond angle, but attempts to verify this by crystallizing them failed. Also, the *p*-nitrophenolate complex [Fe(L11)(H_2O)Cl] **11** exhibits a distorted octahedral coordination geometry with significantly high Fe−O−C bond angles (135.3, 135.6°, Figure 3). However, the five-coordinate complex [Fe(L12)Cl] **12** containing a -NMe_2 group (Figure 3) exhibits a Fe−O−C bond angle of 122° because of the electron-releasing 3,5-dimethylphenolate pendant donors.[27] Thus, iron(III)-phenolate complexes with a sterically hindering -NMe_2 arm contain a Fe−O−C bond angle and Fe−O−C−C dihedral angle as in the 3,4-PCD enzyme, and those with an electron-releasing 3,5-dimethylphenolate/*N*-methylimidazolyl donor display shorter Fe−$O_{phenolate}$ bond.

Electronic Absorption Spectra. In methanol solution all the complexes **1**−**6** exhibit an intense ligand-based band in the range 250−284 nm and two relatively less intense bands (Figure 4, Table 4) in the ranges 329−339 and 536−622 nm, which are assigned[21,27−29,31,51,52] respectively to phenolate (pπ) → Fe(III) (dσ^*) and phenolate (pπ) → Fe(III) (dπ^*) LMCT transitions. The energy of the low energy LMCT band varies as, **1** < **2** > **3**; **4** > **5** > **6**. Obviously, upon replacing a pyridyl moiety in **1** by a more basic *N*-methylimidazolyl moiety to obtain **2**, negative charge is built[26] on iron(III) which raises the iron(III) dπ^* orbital energy, enhances the energy gap between the dπ^* and phenolate (pπ) orbitals, and hence increases the energy of the LMCT band, and so this trend represents a decrease in Lewis acidity of the iron(III) center. A similar increase in the LMCT band energy is observed on replacing the pyridyl moiety in **1** by the strongly σ-bonding -NMe_2 group to obtain **4** (cf. above). However, a similar increase in energy is not observed on going from **2** to **5** and from **4** to **5**. On going from **2** to **3** and **5** to **6** a decrease in energy of the LMCT band is observed. The incorporation of electron-releasing methyl groups at the 3,5-positions in **2** and **5** to obtain **3** and **6**, respectively, raises the energy of the phenolate (pπ) orbital[21a] leading to a decrease in the LMCT band energy. Thus the Lewis acidity of the iron(III) center is fine-tuned by modifying the ligand environment through the replacement of a pyridyl moiety by an imidazolyl moiety and suitable incorporation of methyl groups on the phenolate rings.[45,51]

When the complexes are interacted with DBC^{2-} generated in methanol solution by treating H_2DBC with 2 equiv of Et_3N as base, two new bands in the ranges 466−489 and 676−758 nm appear, which originate from charge transfer from two different catecholate orbitals[20−31,48] on DBC^{2-} chelated to iron(III). The energies of both the DBC^{2-}-to-Fe(III) LMCT bands of [Fe(L)(DBC)] adducts show a remarkable dependence on the nature of the phenolate ligands:[21,22,27−29,48,52,53] [Fe(L3)(DBC)] > [Fe(L2)(DBC)] > [Fe(L1)(DBC)]; [Fe(L6)(DBC)] > [Fe(L5)(DBC)] > [Fe(L4)(DBC)]. This reflects the decrease in Lewis acidity of the iron(III) center, as modified by the primary ligands along these series. Thus upon replacement of the pyridyl moiety as in [Fe(L1)(DBC)] by the more basic *N*-methylimidazolyl moiety as in [Fe(L2)(DBC)], the negative charge built on iron(III) increases and as a result the dπ^* orbitals

(51) (a) Casella, L.; Gullotti, M.; Pintar, A.; Messouri, L.; Rockenbauer, A.; Gyor, M. *Inorg. Chem.* **1987**, *26*, 1031–1038. (b) Wang, S.; Wang, L.; Wang, X.; Luo, Q. *Inorg. Chim. Acta* **1997**, *254*, 71–77. (c) Krebs, B.; Schepers, K.; Bremer, B.; Henkel, G.; Althus, E.; Muller-Warmuth, W.; Griesar, K.; Haase, W. *Inorg. Chem.* **1996**, *35*, 2360–2368. (d) Gaber, B. P.; Miskowski, V.; Spiro, T. G. *J. Am. Chem. Soc.* **1974**, *96*, 6868. (e) Shongwe, M. S.; Kaschula, C. H.; Adsetts, M. S.; Ainscough, E. W.; Brodie, A. M.; Morris, M. J. *Inorg. Chem.* **2005**, *44*, 3070–3079. (f) Imbert, C.; Hratchian, H. P.; Lanznaster, M.; Heeg, M. J.; Hryhorczuk, L. M.; McGarvey, B. R.; Schlegel, H. B.; Verani, C. *Inorg. Chem.* **2005**, *44*, 7414–7422.

(52) Que, L., Jr.; Kolanczyk, R. C.; White, L. S. *J. Am. Chem. Soc.* **1987**, *109*, 5373.

(53) Pyrz, J. W.; Roe, A. L.; Stern, L.; Que, L., Jr. *J. Am. Chem. Soc.* **1985**, *107*, 614–620.

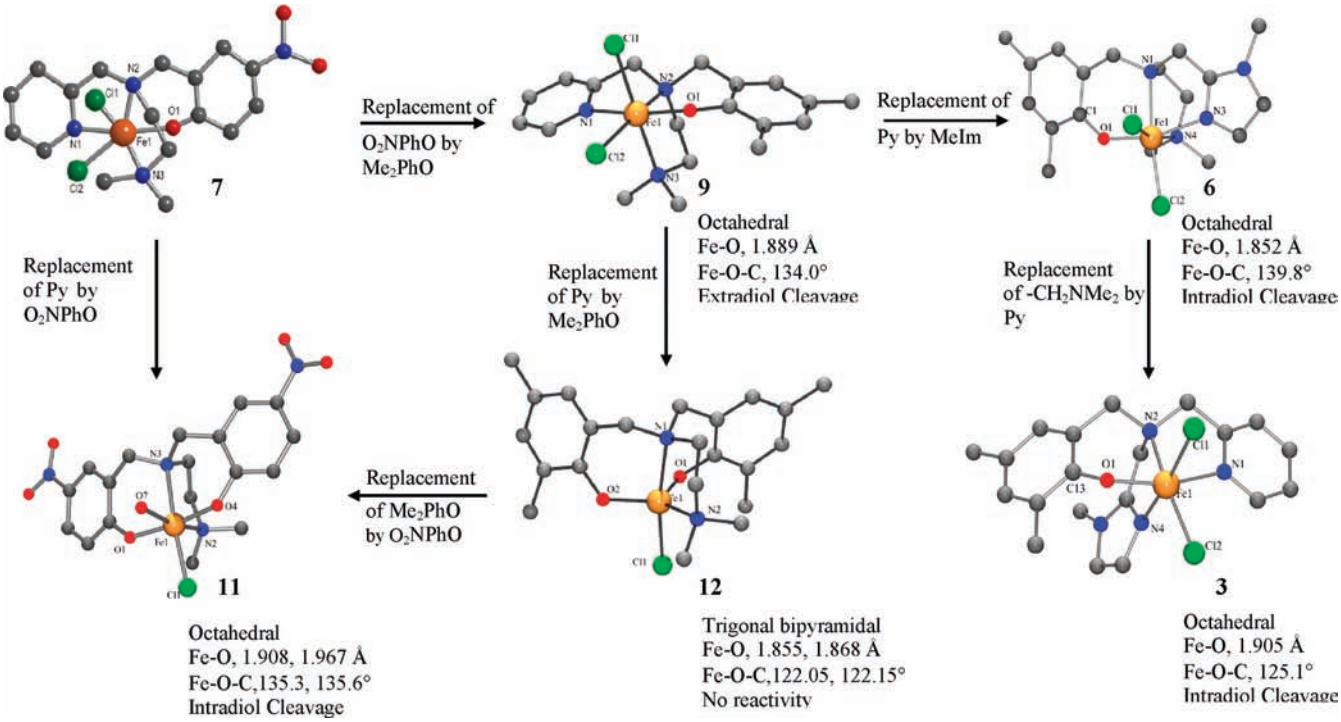

Figure 3. Electronic effects on Iron(III) coordination geometry, Fe−O bond length, and Fe−O−C bond angle and reactivity.

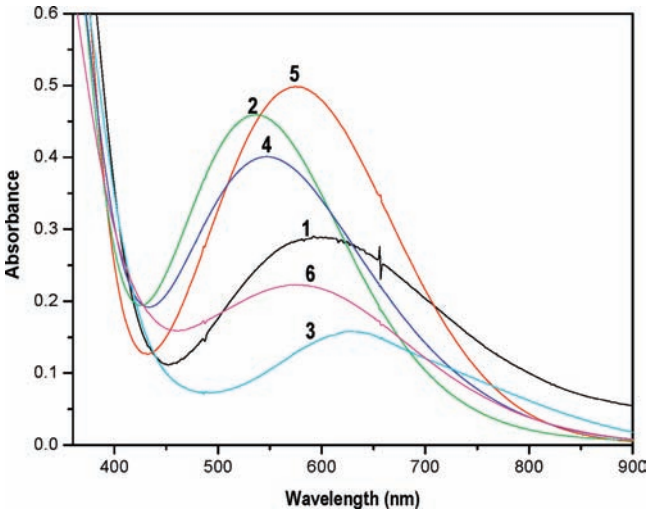

Figure 4. Electronic absorption spectra of iron(III) complexes (2.0×10^{-4} M) in methanol, $[Fe(L1)Cl_2]$ (**1**); $[Fe(L2)Cl_2]$ (**2**); $[Fe(L3)Cl_2]$ (**3**); $[Fe(L4)Cl_2]$ (**4**); $[Fe(L5)Cl_2]$ (**5**); and $[Fe(L6)Cl_2]$ (**6**).

of iron(III) are destabilized[30,48] leading to an increase in energy gap between the dπ* orbital and ligand orbitals and hence the observed increase in the LMCT band energies (cf. above). A similar increase in LMCT band energy is observed on going from [Fe(L2)(DBC)] to [Fe(L3)(DBC)], from [Fe(L4)(DBC)] to [Fe(L5)(DBC)] to [Fe(L6)(DBC)]. However, a small decrease in energy is observed on going from [Fe(L1)(DBC)] to [Fe(L4)-(DBC)]. The position of the low-energy catecholate → Fe(III) LMCT band for the [Fe(L)(catecholate)] adducts generated from **1**−**6** is found to be shifted to higher energies as the substituents[21−24,26−28] on the catecholate ring are varied from electron-releasing to electron-withdrawing:[21] DBC^{2-} > 4-$MCAT^{2-}$ > TBC^{2-} > 3-$MCAT^{2-}$ > CAT^{2-} > TCC^{2-} > 3-$NCAT^{2-}$. This is expected as the electron-releasing substituents on the catecholate ring would decrease, while electron-withdrawing substituents increase the energy of the low energy band,[21−24,26−28] thus reflecting the importance of electronic effects exerted by the substituents on catechols.

Redox Properties. All the complexes show a cathodic and a coupled anodic wave in the Cyclic Voltammogram. The value of diffusion coefficient (D, 2.4−4.8 × 10^{-6} cm^2/s) calculated by substituting the slope obtained from the linear i_{pc} versus $\nu^{1/2}$ (ν < 0.05 V s^{-1}) plot in the Randles−Sevcik equation[54] is of the same order as those observed previously[21,22,27,28] for a one-electron reduction process in similar[28,31] iron(III) complexes. The $E_{1/2}$ values of Fe^{III}/Fe^{II} redox potentials of the present complexes ($E_{1/2}$, −0.205 to −0.317 V, Table 5) follow the trend **1** > **2** > **3**; **4** > **5** > **6**, which represents the decrease in Lewis acidity of the iron(III) center along this series (Supporting Information, Figure S3). Upon replacing one of the pyridylmethyl arms in **1** by a *N*-methylimidazolylmethyl arm to obtain **2**, a very small decrease in $E_{1/2}$ is observed, which is expected of the higher basicity of the *N*-methylimidazole donor. A further but large decrease in $E_{1/2}$ is observed on moving from **2** to **3**; the incorporation of two electron-releasing methyl groups on the phenolate ring enhances the electron density on iron(III) leading to the observed decrease in redox potential. A similar variation in Fe(III)/Fe(II) redox potential along **4**−**6** is observed. Further, on replacing one of the pyridyl moieties in **1** by a $-NMe_2$ group to get **4** the redox potential becomes more negative, which is expected of the strongly σ-bonding $-NMe_2$ group stabilizing iron(III) oxidation state.

(54) Bard, A. J.; Faulkner, L. R. *Electrochemical Methods: Fundamental and Applications*; John Wiley & Sons: New York, 1980; p 218.

Table 4. Electronic Spectral Data, λ_{max}, nm (ε, M^{-1} cm^{-1}) for Iron(III) Complexes[a] and Their Adducts in Methanol

added ligand	$[Fe(L1)Cl_2]$	$[Fe(L2)Cl_2]$	$[Fe(L3)Cl_2]$	$[Fe(L4)Cl_2]$	$[Fe(L5)Cl_2]$	$[Fe(L6)Cl_2]$
none	592 (1 450)	536 (2 300)	622 (1 260)	547 (2 000)	575 (2 500)	585 (1 120)
	329 (4 910)	333 (5 200)	336 (5 430)	339 (4 270)	338 (5 320)	330 (4 050)
	253 (12 625)	279 (8 160)	250 (9 504)	270 (9 090)	275 (8 930)	284 (5 420)
DBC^{2-}	753 (3 045)	720 (2 500)	706 (2 540)	758 (2 830)	718 (2 370)	676 (1 130)
	472 (2 280)	466 (2 690)	477 (1 930)	470 (2 820)	467 (2 630)	489 (1 460)
	287 (10 600)	287 (10 830)	292 (9 990)	286 (10 540)	286 (10 980)	342 (sh)
TBC^{2-}	711 (2 930)	674 (2 630)	693 (1 960)	704 (2 550)	675 (1 760)	639 (sh)
	463 (2 480)	468 (2 890)	292 (9 375)	459 (3 240)	468 (1 830)	331 (sh)
	289 (10 180)	287 (10 900)	245 (11 200)	286 (18 180)	285 (10 170)	287 (8 430)
CAT^{2-}	678 (3 000)	638 (2 520)	639 (2 690)	669 (2 700)	637 (2 030)	573 (1 380)
	459 (2 270)	440 (3 250)	291 (10 150)	455 (3 320)	465 (2 200)	338 (sh)
	285 (11 340)	285 (14 240)	244 (11 130)	285 (14 270)	285 (10 970)	283 (3 755)
TCC^{2-}	627 (3 000)	535 (2 860)	609 (3 603)	609 (2 700)	576 (2 640)	580 (1 820)
	479 (2 300)	307 (7 680)	302 (9 080)	494 (2 690)	306 (7 600)	295 (7 560)
	304 (8 100)	281 (9 090)	248 (14 115)	305 (7 510)	279 (9 010)	
$3\text{-}MC^{2-}$	701 (2 700)	655 (2 520)	644 (2 490)	696 (2 550)	658 (1 900)	584 (1 370)
	475 (2 420)	457 (3 440)	486 (1 920)	472 (2 940)	472 (2 120)	329 (sh)
		284 (13 920)	285 (9 690)	283 (11 240)	284 (10 010)	283 (7 870)
$4\text{-}MC^{2-}$	713 (2 320)	674 (2 220)	655 (2 510)	708 (2 550)	666 (1 780)	613 (1 340)
	463 (2 120)	463 (2 600)	292 (10 180)	466 (2 730)	465 (2 070)	351 (sh)
	291 (10 170)	288 (10 460)	239 (12 000)	288 (10 540)	287 (8 610)	288 (8 370)
$4\text{-}NC^{2-}$	575 (3 490)	511 (4 400)	573 (3 950)	508 (4 580)	520 (3 890)	513 (sh)
	390 (8 620)	403 (9 430)	391 (8 260)	394 (10 950)	402 (7 970)	407 (6 570)
	314 (7 240)	321 (7 140)	265 (14 630)	318 (9 760)	313 (6 620)	329 (6 570)

[a] Concentration of iron(III) complexes, 2×10^{-4} M. The ratio of added ligands to iron(III) complexes, 1:1. The catecholate anions were generated by adding 2 equiv of Et_3N.

A similar decrease in Fe(III)/Fe(II) redox potential is observed on going from **2** to **5** and from **3** to **6**.

On adding 1 equiv of H_2DBC to **1**−**6** in methanol solution no appreciable shift in the Fe(III)/Fe(II) redox potential is observed, and a new DBSQ/H_2DBC redox wave appears ($E_{1/2}$, −0.051 to −0.169 V, Figure 5, Table 5)[21,28,31,48] even in the absence of added base on account of the relatively high Lewis acidity of the iron(III) center in **1**−**6** (Supporting Information, Figure S2). Further, on adding 2 equiv of Et_3N, the intensity of DBSQ/H_2DBC redox wave is increased with a shift in the potential ($E_{1/2}$, −0.039 to −0.147 V).[21,22,27,28,31] The $Fe^{III} \rightarrow Fe^{II}$ reduction process, which is expected[31] to be shifted to more negative potentials on chelation to DBC^{2-}, is difficult to discern as it would have merged with the ligand reduction waves ($E_{1/2}$, −0.325 to −0.640 V). The observed redox potential of DBSQ/H_2DBC couple of coordinated DBC^{2-} (−0.051 to −0.169 V) is less negative than that of free DBSQ/H_2DBC couple (E_{pc}, −1.34 V vs SCE)[55] suggesting stabilization of coordinated DBC^{2-} anion toward oxidation. It is remarkable that the stabilization of catecholate (−0.039 to −0.079 V) is higher for the adducts of pyridyl based complexes **1**, **2**, and **4** than that for the respective adducts of -NMe_2 based complexes **3**, **5**, and **6** (−0.101 to −0.147 V). This means that the electron-transfer[15,48] from catecholate adducts to dioxygen is thermodynamically less favorable for **1**−**3** than for **4** and **5** obviously on account of the higher Lewis acidity of iron(III) centers in the former. Also, a plot of the $E_{1/2}$ of Fe(III)/Fe(II) redox couple versus that of DBSQ/DBC^{2-} redox couple of **1**− **6**, **9**, and **12** gives a straight line (Supporting Information, Figure S2). This reveals that the redox potentials of both couples can be used to illustrate the variation in dioxygenase activity of the complexes and that the ligand donor atoms tune the electronic properties of the iron(III) center not only in the complex but also in the catecholate adducts.

Catechol Dioxygenase Activity of Iron(III) Complexes. The oxygenation reactions for the iron(III) complexes **1**−**6** were carried out using 3,5-di-*tert*-butylcatechol (H_2DBC) as the model substrate, and the advantages of using the latter as substrate are the relatively high stability of the main cleavage product and the fast reaction of the catecholate complexes with dioxygen at room temperature. The DBC^{2-} adducts of **1**−**6** were generated in situ in methanol solution, and their reactivity toward O_2 was investigated by monitoring the decay of the low energy DBC^{2-}-to-Fe(III) LMCT band (Figure 6). The rate constant (k_{obs}) was calculated by fitting the decrease in intensity of the band into the following equation[31,56] applicable for relatively slow reactions,

$$A = A_\infty + (A_0 - A_\infty) \exp(-k_{obs} t) \quad (1)$$

where t is time, A, A_0, and A_∞ are the absorbances at time t, 0, and ∞, respectively, and k_{obs} is the pseudo-first order

(55) Nanni, E. J.; Stalling, M. D.; Sawyer, D. T. *J. Am. Chem. Soc.* **1980**, *102*, 4481–4485.

(56) Hitomi, Y.; Yoshida, M.; Higuchi, M.; Minami, H.; Tanaka, T.; Funabiki, T. *J. Inorg. Biochem.* **2005**, *99*, 755–763.

Table 5. Electrochemical Data[a] for the Iron(III) Complexes and Its DBC^{2-} Adduct[b] in Methanol at 25 ± 0.2 °C Using a Scan Rate of 50 mV/s (CV) and 1 mV/s (DPV)

compound	E_{pc} (V)	E_{pa} (V)	ΔE_p (mV)	$E_{1/2}$ (V) CV	$E_{1/2}$ (V) DPV	redox process
$[Fe(L1)Cl_2]$	−0.260	−0.126	134	−0.193	−0.205	$Fe^{III} \rightarrow Fe^{II}$
+ H_2DBC	−0.236				−0.177	$Fe^{III} \rightarrow Fe^{II}$
	−0.092	−0.008	84	−0.050	−0.051	$DBSQ \rightarrow H_2DBC$
+ DBC^{2-}	−0.674	−0.542	132	−0.608	−0.600	$Fe^{III} \rightarrow Fe^{II}$ + LR
	−0.088	0.024	64	−0.032	−0.039	$DBSQ \rightarrow H_2DBC$
$[Fe(L2)Cl_2]$	−0.262	−0.118	144	−0.190	−0.209	$Fe^{III} \rightarrow Fe^{II}$
+ H_2DBC	−0.250	−0.156	94	−0.203	−0.205	$Fe^{III} \rightarrow Fe^{II}$
	−0.080				−0.047	$DBSQ \rightarrow H_2DBC$
+ DBC^{2-}	−0.634	−0.534	100	−0.584	−0.598	$Fe^{III} \rightarrow Fe^{II}$ + LR
	−0.126	−0.026	100	−0.076	−0.079	$DBSQ \rightarrow H_2DBC$
$[Fe(L3)Cl_2]$	−0.372	−0.238	134	−0.305	−0.317	$Fe^{III} \rightarrow Fe^{II}$
+ H_2DBC	−0.386	−0.234	152	−0.310	−0.313	$Fe^{III} \rightarrow Fe^{II}$
	−0.080				−0.169	$DBSQ \rightarrow H_2DBC$
+ DBC^{2-}	−0.378	−0.268	110	−0.323	−0.325	$Fe^{III} \rightarrow Fe^{II}$
	−0.202	−0.082	120	−0.142	−0.147	$DBSQ \rightarrow H_2DBC$
$[Fe(L4)Cl_2]$	−0.288	−0.202	86	−0.245	−0.235	$Fe^{III} \rightarrow Fe^{II}$
+ H_2DBC	−0.272	−0.200	72	−0.236	−0.229	$Fe^{III} \rightarrow Fe^{II}$
	−0.092	−0.004	88	−0.048	−0.057	$DBSQ \rightarrow H_2DBC$
+ DBC^{2-}	−0.682	−0.562	120	−0.622	−0.625	$Fe^{III} \rightarrow Fe^{II}$ + LR
	−0.100	−0.004	96	−0.052	−0.049	$DBSQ \rightarrow H_2DBC$
$[Fe(L5)Cl_2]$	−0.324	−0.214	110	−0.269	−0.273	$Fe^{III} \rightarrow Fe^{II}$
+ H_2DBC	−0.328	−0.218	110	−0.273	−0.283	$Fe^{III} \rightarrow Fe^{II}$
	−0.186	−0.046	140	−0.116	−0.117	$DBSQ \rightarrow H_2DBC$
+ DBC^{2-}	−0.692	−0.564	128	−0.628	−0.640	$Fe^{III} \rightarrow Fe^{II}$ + LR
	−0.160	−0.056	104	−0.108	−0.101	$DBSQ \rightarrow H_2DBC$
$[Fe(L6)Cl_2]$	−0.340	−0.280	60	−0.310	−0.313	$Fe^{III} \rightarrow Fe^{II}$
+ H_2DBC	−0.348	−0.278	70	−0.313	−0.325	$Fe^{III} \rightarrow Fe^{II}$
	−0.086	−0.016	70	−0.051	−0.061	$DBSQ \rightarrow H_2DBC$
+ DBC^{2-}	−0.678	−0.567	111	−0.622	−0.625	$Fe^{III} \rightarrow Fe^{II}$
	−0.172	−0.063	109	−0.117	−0.111	$DBSQ \rightarrow H_2DBC$

[a] Potential measured vs $Ag/AgNO_3$ (0.01 M, 0.1 M TBAP); add 0.544 V to convert to NHE. [b] Generated by adding 2 equiv triethylamine to H_2DBC.

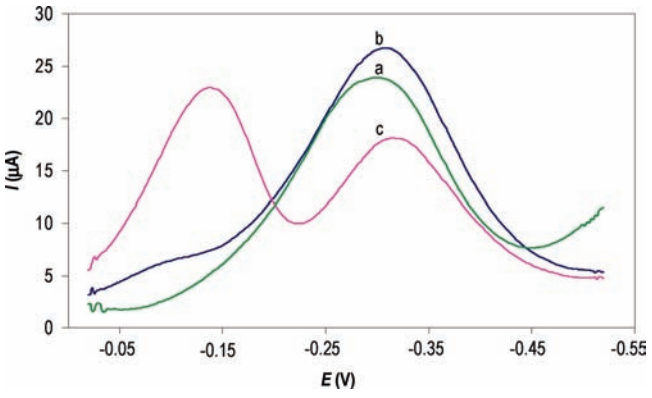

Figure 5. Differential pulse voltammograms of 1 mM $[Fe(L3)Cl_2]$ before (a) and after addition of 1 mM H_2DBC (b) and 2 mM Et_3N (c) in methanol at 25 °C. Supporting electrolyte, 0.1 M TBAP; scan rate, 0.05 V s^{-1}; reference electrode, Ag/Ag^+; working electrode, Pt sphere.

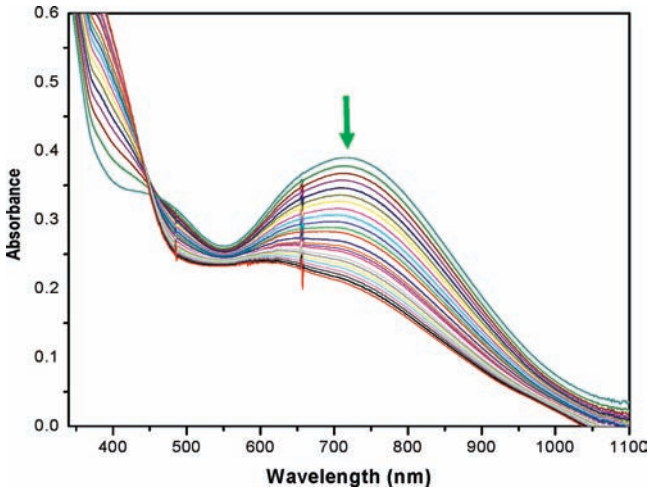

Figure 6. Progress of the reaction of [Fe(L3)(DBC)] (2.0×10^{-4} M) with O_2 in methanol solution by monitoring the disappearance of DBC^{2-}-to-Fe(III) LMCT band at 720 nm.

rate constant. The $t_{1/2}$ of the catecholate adducts were calculated[31] using the equation $t_{1/2} = 0.693/k_{obs}$. The second order rate constants ($k_{O_2} = k_{obs}/[O_2]$) of the reactions were then derived[24,37] (Table 6) by incorporating the concentration of O_2 in methanol as 2.12×10^{-3} M.[24,37]

The in situ generated adducts [Fe(L)(DBC)] of complexes **1**−**6** were reacted with dioxygen over 48 h ($t_{1/2}$: 4.0−16.4 h) to afford intradiol cleavage products (13.6−55.3%) almost exclusively with very small amounts of extradiol products for **2** (3.6%) and **6** (5.4%, Scheme 3, Table 6). The oxygenation products were identified by GC-MS (EI) and ^1H NMR and quantified by GC (FID) techniques. The oxidative intradiol cleavage product 3,5-di-*tert*-butyl-5-(carboxymethyl)-2-furanone, $C_{15}H_{24}O_4$, *m*/*z*, 254, **13** (13.3−43.6%) (Scheme 3, Table 6) is obtained in major amounts. The intradiol product **13** is derived[52] from the nucleophilic attack of hydroxide ion on *cis*,*cis*-muconic anhydride, which is the immediate product of oxidative cleavage. Small amounts of two isomeric extradiol cleavage products ($C_{13}H_{20}O_2$, *m*/*z*, 208) 3,5-di-*tert*-butyl-2-pyrone **14** (0.5−5.4%) and 4,6-di-*tert*-butyl-2-pyrone **15** (1.8%) resulting from the

Table 6. Kinetic Data for the Oxidative Cleavage of H_2DBC Catalyzed by Iron(III) Complexes in Methanol and the Cleavage Products Analyzed after 48 h (See Scheme 3)

	cleavage products (%)[b]				
complex[a]	intradiol	extradiol	k_{obs} (10^{-5} s^{-1})	k_{O_2} (10^{-2} M^{-1} s^{-1})[c]	$t_{1/2}$ (h)[d]
$[Fe(L1)Cl_2]$	43.6 (**13**)	0.5 (**14**)	1.18 ± 0.01	0.56 ± 0.05	16.4
$[Fe(L1)(MeOH)_2]^{2+}$	33.1 (**13**)		2.35 ± 0.07	1.11 ± 0.01	8.2
$[Fe(L2)Cl_2]$	32.7 (**13**)	3.6 (**14**)	2.93 ± 0.12	1.39 ± 0.06	6.7
$[Fe(L2)(MeOH)_2]^{2+}$	32.2 (**13**)	3.9 (**14**)	1.96 ± 0.14	1.86 ± 9.8	8
$[Fe(L3)Cl_2]$	30.1 (**10**)		14.72 ± 0.36	6.9 ± 0.17	1.3
$[Fe(L3)(MeOH)_2]^{2+}$	28.3 (**13**)		6.24 ± 0.09	2.9 ± 0.04	3.1
$[Fe(L4)Cl_2]$	55.3 (**13**)	0.4 (**14**)	3.57 ± 0.09	1.69 ± 0.04	5.4
$[Fe(L4)(MeOH)_2]^{2+}$	32.0 (**13**)		2.83 ± 0.03	1.33 ± 0.02	6.8
$[Fe(L5)Cl_2]$	50.6 (**13**)	0.8 (**14**)	4.85 ± 0.21	2.29 ± 0.10	4.0
$[Fe(L5)(MeOH)_2]^{2+}$	35.5 (**13**)		3.94 ± 0.17	0.93 ± 0.07	4.9
$[Fe(L6)Cl_2]$	13.3 (**13**)	5.4 (**14, 15**)	2.15 ± 0.16	1.02 ± 0.08	8.9
$[Fe(L6)(MeOH)_2]^{2+}$	32.2 (**13**)	4.9 (**14**)	1.98 ± 0.13	0.93 ± 0.06	9.7

[a] $[Fe(L)(MeOH)_2]^{2+}$ species generated from $[Fe(L)Cl_2]$ by adding 2 equiv of $AgClO_4$. [b] Based on H_2DBC, Piperidine (Pip). [c] $k_{O_2} = k_{obs}/[O_2]$. [d] $t_{1/2} = 0.693/k_{obs}$.

Scheme 3. Oxygenation Products of H_2DBC Catalyzed by Iron(III) Complexes Using Dioxygen

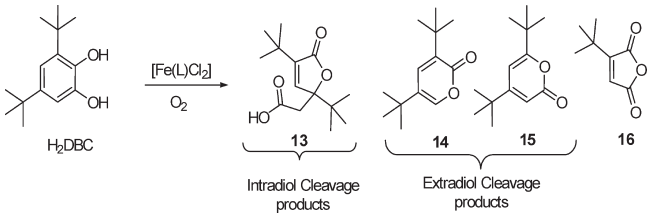

insertion of an oxygen atom of molecular oxygen into H_2DBC followed by loss[57,58] of CO and a minor amount of the side product **16** are obtained.

The formation of intradiol cleavage products for the catecholate adducts of **1**−**6** is expected of their six-coordinate geometry, which favors substrate-activation[16,20,24−26,28,30,31] rather than dioxygen-activation[15,30,48,57−59] pathway as the latter requires a vacant coordination site on the catecholate adduct for oxygen coordination followed by activation. The observation of lower amounts of extradiol products for **2** and **6** may be illustrated by invoking the displacement of the weakly coordinated pyridyl or -NMe_2 arm from the coordination sphere containing more Lewis basic ligand donors, which facilitates dioxygen attack on iron(III) for extradiol cleavage to occur. The displaced pyridyl or -NMe_2 arm might act as an acid−base catalyst proposed for the extradiol-cleavage pathway.[31,60−63]

Que[20,26,30,52] and Palaniandavar[22,28,48] have previously demonstrated that a higher Lewis acidity of the iron(III) center facilitates stronger binding of H_2DBC and hence higher metal-catecholate covalency conferring a higher rate of oxygenation of the substrate. Thus the replacement of one of the two pyridylmethyl arms in $[Fe(TPA)(DBC)]^+$ (k_{O_2}, 1.5×10^3 M^{-1} s^{-1})[20] by a phenolate arm to obtain the adducts [Fe(L1)-(DBC)]−[Fe(L6)(DBC)] decreases the Lewis acidity of the iron(III) center and hence lowers the rate of dioxygenation enormously (k_{O_2}, $5.6-69.0 \times 10^{-3}$ M^{-1} s^{-1}). When the Lewis basicity of the phenolate donor is tuned by incorporating different substituents on the phenolate ring, interesting results are obtained. Thus incorporation of two electron-releasing methyl groups at 3,5-positions on the phenolate arm in **5** to obtain **6** and that in **4** to obtain **9** leads to a decrease in reaction rate, which is expected of the decrease in Lewis acidity of the iron(III) center. Also, a much lower Lewis acidity of the iron(III) center in **6** and **9** would favor regioselective/specific extradiol cleavage contributing to the lower rate of cleavage (cf. above).[31] On the other hand, a similar substitution on the phenolate ring in **2** to obtain **3** leads to an increased reaction rate (cf. below). Also, incorporation of electron-withdrawing nitro group on the phenolate moiety in **4** to obtain [Fe(L7)Cl] **7** slightly decreases[28] the reaction rate while that in **5** to obtain [Fe(L8)Cl] **8** (Figure 3) slightly increases the reaction rate.[28] In this regard it is to be noted that incorporation of *p*-nitro substituent on the phenolate ring as in $[Fe(L10)Cl_2]$ **10** leads to lack of reactivity toward dioxygen and H_2O_2 as well.[28,64] Also, incorporation of two 3,5-dimethylphenolate arms as in [Fe(L12)Cl] **12** leads to no dioxygenase activity while that of two *p*-nitrophenolate arms as in $[Fe(L10)(H_2O)Cl]$ **11** confers dioxygenase activity (k_{O_2}, 3.76×10^{-3} M^{-1} s^{-1},) illustrating the significance of the higher Fe−O−C bond angles in the latter[22] (Figure 3).

When the pyridyl moiety in **1** and **4** is replaced by the more basic *N*-methylimidazolyl moiety to obtain **2** and **5**, respectively, the dioxygenation rate is expected to decrease because of the decrease in Lewis acidity of the iron(III) center (cf. above). But, interestingly, the rates observed for **2** and **5** are respectively higher than those for **1** and **4**; this suggests that the sterically low demanding *N*-methylimidazolyl moiety facilitates the binding of catechol substrate to iron(III) and the approach of molecular

(57) Ito, M.; Que, L., Jr. *Angew. Chem., Int. Ed. Engl.* **1997**, *36*, 1342–1344.
(58) (a) Funabiki, T.; Mizoguchi, A.; Sugimoto, T.; Tada, S.; Tsuji, M.; Sakamoto, H.; Yoshida, S. *J. Am. Chem. Soc.* **1986**, *108*, 2921–2932. (b) Funabiki, T.; Mizoguchi, A.; Sugimoto, T.; Yoshida, S. *Chem. Lett.* **1983**, 917–920.
(59) Die, A.; Gatteschi, D.; Pardi, L. *Inorg. Chem.* **1993**, *32*, 1389–1395.
(60) Winfield, C. J.; Al-Mahrizy, Z.; Gravestock, M.; Bugg, T. D. H. *J. Chem. Soc., Perkin Trans. 1* **2000**, 3277–3289.
(61) Mendel, S.; Arndt, A.; Bugg, T. D. H. *Biochemistry* **2004**, *43*, 13390–13396.
(62) Jo, D.-H.; Chiuo, Y.-M.; Que, L., Jr. *Inorg. Chem.* **2001**, *40*, 3181–3190.
(63) Mayilmurugan, R.; Evans, H. S.; Palaniandavar, M. *Inorg. Chem.* **2008**, *47*, 6645–6658.
(64) Nishida, Y.; Shimo, H.; Kida, S. *J. Chem. Soc., Chem. Commun.* **1984**, 1611–1612.

oxygen as well. However, lower amounts of intradiol cleavage products are observed for **2** and **5** (**2**, 32.7; **5**, 50.6%) than those, respectively, for **1** and **4** (**1**: 43.6; **5**, 55.3%) because of decreased Lewis acidity of the iron(III) center in forming lower amounts of catecholate adducts. Similar enhanced reaction rates and yields have been observed previously for iron(III) complexes of imidazole-based tripodal $4N$[24] and N_3O(monophenolate)[28] ligands. Also, on replacing one of the pyridyl moieties in **1** and **2** by the more basic -NMe_2 pendant to obtain **4** and **5**, the lower Lewis acidity conferred on the iron(III) center in the latter complexes (cf. above) would be expected to decrease the rate of dioxygenation. But, interestingly, an enhancement in rates is observed, which is consistent with the higher amounts of intradiol products observed for **4** and **5** (**4**: 55.3; **5**, 50.6%) than for **1** and **2**, respectively (**1**: 43.6; **2**, 32.7%). It is possible that incorporation of the sterically demanding -NMe_2 pendant would enhance the Fe−O−C bond angle (cf. above), resulting in increase in iron(III)-catecholate covalency and hence enhancement in dioxygenase activity. A similar enhanced reactivity upon incorporation of sterically demanding −NMe_2 donor in iron(III)-monophenolate complexes with high Fe−O−C bond angle has been observed by us previously (Figure 3).[28] However, interestingly, a decrease in rate of dioxygenation is observed upon replacing the pyridyl moiety in **3** by the -NMe_2 pendant to obtain **6** in spite of the higher Fe−O−C bond angle and shorter Fe−O bond length observed for **6** (cf. above, Figure 3). The lower reactivity is possibly due to the lower Lewis acidity of the iron(III) center in **6** and is consistent with the extradiol cleavage activity observed. No systematic changes in reaction rates are observed upon solvation for all the present complexes.

Funabiki et al. have investigated the dioxygenation of octahedral [Fe(TPA)(R-Cat)]BPh_4 adducts, where R-Cat are differently substituted catechols, with O_2 and invoked a spin-inversion phenomenon to illustrate the LMCT energy-dependent reactivity, an adduct with a low-energy catecholate-to-iron(III) LMCT band exhibiting a higher rate of dioxygenase activity.[56] Very recently, a similar linear correlation has been observed[48] for [Fe(L)(DBC)(Sol)]$^+$ (L = 3N *cis*-facial ligands; Sol = Solvent). For the present adducts also the plot of $\log(k_{O_2})$ versus energy of the low-energy catecholate-to-iron(III) LMCT band (Figure 7) tends to be linear; however, in contrast to the above 3N ligand complexes, it is seen that among **1**−**5** the rate of dioxygenation increases with increase in the LMCT band energy. A similar increase in rate with increase in $Cat^{2-} \rightarrow$ Fe(III) LMCT band has been observed by Krebs et al. for octahedral iron(III) complexes of tripodal tetradentate 4N ligands.[24] It appears that the difference in reactivity is possibly because the catecholate adducts of tridentate 3N ligand complexes[48] contain a vacant (solvated) site, which facilitates concerted dioxygen attack on both the activated catecholate and iron(III) site leading to peroxy adduct formation and hence intradiol cleavage[65] while those of the present six-coordinate complexes do not encourage a concerted attack of dioxygen. So dioxygen would first attack a carbon site on

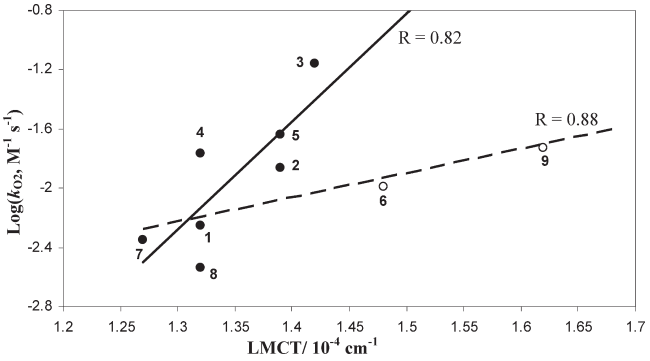

Figure 7. Plot of logarithm of the second-order reaction rate constant versus the energy of the lower-energy LMCT band of [Fe(L)(DBC)] derived from **1**−**7** and **9** in methanol and **8** in acetonitrile solution.

the octahedral iron(III)-bound catecholate and then bind to the iron(III) center after or before displacing the weakly coordinated -NMe_2 donor group forming, respectively, a six- or seven-coordinate[56] peroxo intermediate, which, after Criegee rearrangement followed by solvent attack, yields the product and regenerates the complex. The lower reaction rates observed for the adducts [Fe(L6)(DBC)] and [Fe(L9)(DBC)][31] (Figure 3) may be because both the intra- and the extradiol cleavage pathways contribute to the observed rates, as illustrated above for **6**. In fact, it is interesting to note that the catecholate adducts of **6**, **7**,[28] and **9**, all with higher Fe−O−C bond angle, lie on another straight line along with **1** and **2** and that the rate of dioxygenation of these complexes also increases with increase in the LMCT band energy.

Also, a plot of $\log(k_{O_2})$ versus the $E_{1/2}$ of DBSQ/DBC^{2-} redox couple ($E_{1/2}$, −0.039 to −0.147 V; ΔE_p, 64−120 mV, cf. above; Figure 8; Supporting Information, Figure S4) tends to be linear, and, interestingly, complex **3** with the most negative redox potential for the DBSQ/DBC^{2-} couple and a higher value of the $DBC^{2-} \rightarrow$ Fe(III) LMCT band among the present complexes (cf. above) shows the highest rate of reaction. Also, the complexes **4** and **5** with more negative redox potentials for DBSQ/DBC^{2-} react faster than **1** and **2**, respectively.

Thus it is clear that a more negative DBSQ/DBC^{2-} redox potential for a complex would correspond to a stronger iron(III)-catecholate covalency leading to a higher reaction rate. All these observations can be elegantly illustrated by invoking the mechanism proposed very recently by Solomon et al.[65] to overcome the spin-forbidden nature of the reaction between the triplet O_2 and spin singlet of the organic substrate. The enzyme−substrate (ES) complex of intradiol catechol dioxygenase reacts with molecular oxygen to form the intermediate ESO_2 complex with $S = 3/2$ spin, and both the iron center and the catecholate substrate are activated by a low energy catecholate-to-iron(III) charge transfer transition in this highly covalent ES complex. Thus, the intradiol cleavage of coordinated PCA involves a very low energy β-electron transfer from the frontier (highest occupied) molecular orbital ($\pi_{op\text{-}sym}$) of iron(III)-bound substrate to the iron(III) center ($S = 5/2$, 5 α spins) and the high energy α-electron transfer to π_{ip} orbital of the O_2 molecule containing a β-electron, which enables electrophilic attack by the O_2 molecule. In turn, the α spin in iron(III) center is transferred to the π_{op} orbital of the

(65) Pau, M. Y. M.; Lipscomb, J. D.; Solomon, E. I. *Proc. Natl. Acad. Sci. U.S.A.* **2007**, *104*, 18355–18362.

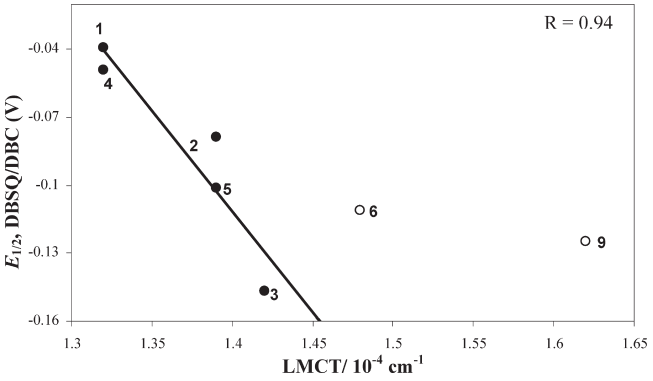

Figure 8. Plot of redox potential of DBSQ/DBC couple versus the energy of LMCT band of [Fe(L)(DBC)] derived from **1**− **6** and **9** in methanol solution.

O_2 molecule containing the other β-electron through a strong π overlap between the d_{xz} orbital of iron(III) with the π^* orbital of the O_2 molecule. So the rate of dioxygenation would be dependent also upon the energy needed for the β-electron transfer, a lower energy for the corresponding LMCT transition leading to faster electron transfer as observed for the above octahedral catecholate adducts of iron(III) complexes of 3N ligands. However, for **3** showing the highest reaction rate among the present complexes, the LMCT band is observed at a higher energy. It appears that the transfer of α spin in the d_{xz} orbital of iron(III) to the O_2 molecule is facilitated in this complex as this orbital is destabilized[65] because of accumulation of electron density on iron(III) by the strongly electron-releasing 3,5-dimethylphenolate donor. This is supported by the more negative redox potential of the DBSQ/DBC^{2-} redox couple, which means a higher electron density built on iron(III) leading to the facile transfer of α spin of iron(III) directly to molecular oxygen upon its forming the peroxo bond with iron(III). Also, a more negative redox potential for the DBSQ/DBC^{2-} redox couple would mean a facile removal of electrons from the catecholate substrate. A similar explanation can be extended to complexes **4** and **5** with more negative potentials for the DBSQ/DBC^{2-} redox couple but with almost the same LMCT band energy. Also, the present observation reveals the importance of substrate activation mechanism of intradiol cleavage and the use of the $E_{1/2}$ value of DBSQ/DBC^{2-} redox couple of bound catecholate rather than that of Fe(III)/Fe(II) redox couple in illustrating the dioxygenase activity.

Thus, when the substituents on the phenolate arm are varied to decrease the Lewis acidity of the iron(III) center, the reaction rate decreases. And, interestingly, when the Lewis acidity of the iron(III) center is decreased further by incorporating the 3,5-dimethylphenolate arm, extradiol cleavage product is also observed. When the electron-releasing but sterically low demanding *N*-methylimidazolyl moiety is incorporated in the iron(III) coordination sphere to decrease the Lewis acidity, the reaction rate is enhanced. On the other hand, when the sterically demanding -NMe_2 group is used to decrease the Lewis acidity of iron(III), the reaction rate is increased. It is obvious that the enhanced interaction of the catecholate substrate with iron(III) in the catecholate adduct rather than the Lewis acidity of the iron(III) center in the complex, as determined by the substituents on the phenolate ring and the steric and electronic effects of other ligand donors, dictates the nature and amount of cleavage products and the rate of dioxygenation as well for the iron(III)-monophenolate complexes. It is to be cautioned that the existence of multiple reaction pathways for the present small molecule analogues is difficult to disregard at this stage. Also, the present study illustrates the role of iron(III)-tyrosinate/imidazole coordination in catechol dioxygenases. It is clear that the interplay of several factors, namely, the Lewis acidity of the enzyme−substrate adduct rather than that of the iron(III) center in the enzyme and steric hindrance of donor groups toward oxygen attack are critically tuned in the enzymes to result in an efficient and facile intradiol cleavage of the catecholate substrate.

Conclusions

To conclude, a series of new mononuclear octahedral iron(III) complexes of tripodal monophenolate ligands offering a N_3O donor set have been isolated and studied as structural, spectral, and functional models for the intradiol-cleaving catechol dioxygenase enzymes. Upon replacing the pyridyl moiety in one of the complexes containing *N*-methylimidazolyl moiety by a $-CH_2NMe_2$ group the Fe−O−C bond angle increases from 125.1° to 139.8°, but, interestingly, decreased intradiol cleavage along with extradiol cleavage activity, is observed. Interestingly, the higher Fe−O−C bond angle observed for the complex is similar to that in the 3,4-PCD enzyme (Fe−O−C, 133, 148°). The rate of intradiol dioxygenase reaction has been correlated with the energy of the low energy catecholate-to-iron(III) LMCT band, a higher value corresponding to a higher rate of dioxygenation, as well as the redox potential of DBSQ/DBC^{2-} couple of iron(III)-bound catecholate substrate, a more negative value corresponding to a higher rate of cleavage of catechol. Thus, the different substituents on the coordinated phenolate ring and the nature of the nitrogen donor function, pyridine/*N*-methylimidazole/-NMe_2, on the other arms of the tripodal monophenolate ligands dictate the stereo-electronic properties and also the catechol cleavage activity of the iron(III) complexes.

Acknowledgment. We sincerely thank the Department of Science and Technology, New Delhi, for supporting this research [Scheme No. SR/S1/IC-45/2003, SR/S5/BC-05/2006], and the Council of Scientific and Industrial Research, New Delhi for Senior Research Fellowships to R.M. and K.V. Professor M. Palaniandavar is a recipient of a Ramanna Fellowship of the Department of Science and Technology, New Delhi. We thank Professor P. Sambasiva Rao, Pondicherry University, for providing the EPR facility.

Note Added after ASAP Publication. This paper was published ASAP on August 20, 2009 with an error in Figure 3. The corrected version was published ASAP on September 14, 2009.

Supporting Information Available: Correlation plots and crystallographic data in CIF format for **3** and **6**. This material is available free of charge via the Internet at http://pubs.acs.org.